

A semi-empirical dynamic soil acidification model for use in spatially explicit integrated assessment models for Europe

A semi-empirical dynamic soil acidification model for use in spatially explicit integrated assessment models for Europe

**Gert Jan Reinds
Maximilian Posch (RIVM/CCE)
Wim de Vries**

Alterra-rapport 084

Alterra, Green World Research, Wageningen, 2001

ABSTRACT

Reinds, G.J, M. Posch and W. de Vries, 2001. A semi-empirical dynamic soil acidification model for use in spatially explicit integrated assessment models for Europe. Wageningen, Alterra, Green World Research. Alterra-rapport 084, 56 blz. 9 fig.; 10 tab.; 41 ref.

A semi-empirical soil acidification model was developed for use in integrated assessment models on a European scale. The model simulates the time development of base-saturation and aluminium concentration using an empirical relationship with pH. An accompanying data set was developed by overlaying European maps on soils, land-use, climate and altitude followed by a procedure that aggregates the input data over soil-texture combinations in each EMEP 150 x 150 km grid cell. Model tests show that the model gives results comparable to the SMART model although it overestimates initial base saturation in some areas with high acid input and simulates a faster recovery from acidification than SMART.

Keywords: Soil acidification, Dynamic Modelling, Europe

ISSN 1566-7197

Dit rapport kunt u bestellen door NLG 40,00 over te maken op banknummer 36 70 54 612 ten name van Alterra, Wageningen, onder vermelding van Alterra-rapport 084. Dit bedrag is inclusief BTW en verzendkosten.

© 2001 Alterra, Green World Research,
P.O. Box 47, NL-6700 AA Wageningen (The Netherlands).
Phone: +31 317 474700; fax: +31 317 419000; e-mail: postkamer@alterra.wag-ur.nl

No part of this publication may be reproduced or published in any form or by any means, or stored in a data base or retrieval system, without the written permission of Alterra.

Alterra assumes no liability for any losses resulting from the use of this document.

Alterra is the amalgamation of the Institute for Forestry and Nature Research (IBN) and the Winand Staring Centre for Integrated Land, Soil and Water Research (SC). The merger took place on 1 January 2000.

Project 020-10545

[Alterra-rapport 084/IS/03-2001]

Contents

Preface	7
Summary	9
1 Introduction	11
2 Model conceptualisation	13
2.1 Basic equations	13
2.2 Empirical relationships between base saturation and pH	14
2.3 Summary of model and input data required	17
3 Input data	19
3.1 Map overlays	19
3.2 Input data for the model	23
4 Model results	31
5 Discussion and conclusions	35
References	37
Annexes	
1 FAO soil types in Europe	41
2 Site quality estimates	45
3 Yield tables	47
4 Evapotranspiration and Soil Moisture Calculations	53

Preface

This report contains a description of a semi-empirical soil acidification model that was developed for the Environmental Economics Group of the Department of Economics and Management of Wageningen UR for use in their integrated assessment model for optimization of emission abatement strategies. The work was partly financed by the Coordination Center For Effects of RIVM (RIVM/CCE) within the context of the cooperation between RIVM/CCE and Alterra on dynamic modeling.

Summary

Dynamic soil acidification models, such as SMART, have been designed for use on a regional scale but are still too complex to be used in the optimisation mode of regional integrated economic assessment models such as RAINS. Therefore a very simple semi-empirical soil acidification model was developed for use in such a dynamic optimisation of pollution reduction costs. The resulting model consists of a set of three equations that relate sulphur and nitrogen deposition (the driving forces) to effects on the soil solution characterised by, e.g., pH or aluminium concentration. Instead of a process-oriented description of cation exchange (used, e.g., in SMART), the time development of the base saturation is described by empirical relationships with pH for four soil texture classes. These relationships were based on numerous simulations with the SMART model. Results indicate clear relationships between these two parameters for soil texture classes 'coarse' and 'medium', which cover about 80% of all European forest soils.

A map with computation units for Europe was constructed by overlaying maps with geo-referenced information on soils, forest, climate and altitude. The resulting map consists of about 100000 computation units (forest soils). For the optimisation model, a generalised data set was derived by aggregating input data for the semi-empirical model over combinations of soil group and texture class in each EMEP 150-km grid cell. The resulting data set consists of about 1400 computation units.

The semi-empirical model was tested by comparing its output on a European scale with results from the SMART model. Results show that some differences exist between the outcome of the models, and that on a European scale the semi-empirical model simulates a faster recovery (in terms of aluminium concentration) of soils than SMART with the same acid input. It therefore might give reasonable results for short simulation periods, but might give deviating results for longer time periods. However, instead of finetuning the semi-empirical model, future developments will concentrate on simplifying SMART into a very simple process-based dynamic soil acidification model.

1 Introduction

Although dynamic soil acidification models such as SMART (De Vries et al., 1989; Posch et al., 1993) have been designed for use on a regional scale (De Vries et al., 1994), requiring the simulation of many thousand of sites, this type of model was found too complex to be used in the optimisation mode of regional integrated economic assessment models such as RAINS (Alcamo et al., 1990) or similar models (Schmieman and Ierland, 1999), since it needs to compute soil (solution) properties many times for a single site alone in the course of finding the optimal timing of emission reductions. Therefore a very simple semi-empirical soil acidification model was developed for use in dynamic optimisation of pollution reduction costs in a regional integrated economic assessment (Schmieman et al., 2000).

The model describes the time development of the base saturation of a soil where the link to soil solution variables is modelled by an empirical relationship with pH. This relationship has been derived from a large number of simulations with the SMART model using a European soil database.

The resulting model consists of a set of three equations that relate sulphur and nitrogen deposition (the driving forces) to effects on the soil solution, characterised by, e.g., pH or aluminium concentration. By using thresholds for these soil chemical values, it thus can be used as a tool for evaluating emission reduction alternatives in terms of ecosystem protection.

2 Model conceptualisation

2.1 Basic equations

In this chapter the semi-empirical soil acidification model is derived. Since we are interested only in long-term (slow) changes in the status of the soil, we can restrict ourselves to the time development of the number of sites at the exchange complex of the soil matrix occupied by base cations, which can be exchanged with protons and/or aluminium ions. This number of sites is given by $b \times CEC_a$, where CEC_a is the areal cation exchange capacity of the rooting zone (a soil property) and $b=b(t)$ is the so-called base saturation, the fraction of the cation exchange capacity occupied by base cations at time t ($0 \leq b(t) \leq 1$). The mass balance of the base cations in the soil/soil solution system is given by:

$$CEC_a \cdot \frac{db}{dt} = BC_{in} - BC_{le} \quad (1)$$

where BC_{in} ($\text{eq.m}^2.\text{yr}^{-1}$) is the net input of base cations ($BC=Ca+Mg+K+Na$) and BC_{le} is the leaching of base cations from the root zone. The concentration of base cations is influenced by the deposition of acidifying sulphur (S) and nitrogen (N) via the charge balance, which has to hold for the leaching flux from the root zone:

$$SO_{4,le} + N_{le} + Cl_{le} - BC_{le} = H_{le} + Al_{le} - HCO_{3,le} - RCOO_{le} = Ac_{le} \quad (2)$$

where RCOO stands for the sum of organic anions and where we have defined Ac_{le} , the leaching of acidity. The leaching of chloride, Cl_{le} is assumed equal to the chloride deposition Cl_{dep} . Neglecting sulphur sources and sinks in the soil, the leaching of sulphate equals its deposition:

$$SO_{4,le} = S_{dep} \quad (3)$$

Sulphate ad/desorption is a slow process; and if it cannot be neglected, the model presented here is not applicable, and would have to be extended to include it. For nitrogen the balance reads:

$$N_{le} = f_{net} \cdot N_{dep} - N_u \quad (4)$$

where f_{net} is a fraction accounting for denitrification and N-immobilisation ($0 \leq f_{net} \leq 1$) and N_u is the net growth uptake of nitrogen. We assume complete nitrification, i.e. N_{dep} is the sum of NO_x and NH_3 deposition. For base cations the net input is given as:

$$BC_{in} = BC_{dep} + BC_{we} - BC_u \quad (5)$$

where the subscripts *dep*, *we* and *u* stand for deposition, weathering and net uptake, respectively.

Defining the free aluminium concentration as the total aluminium concentration minus the concentration of organic anions, the leaching of acidity is defined as the leaching of protons, free aluminium and bicarbonate, i.e.

$$Ac_{le} = Q \cdot ([H] + [Al] - [HCO_3]) \quad (6)$$

where Q ($m \cdot yr^{-1}$) is the percolating water (precipitation surplus) and the square brackets denote concentrations (in $eq \cdot m^{-3}$). The concentration of free aluminium (not complexed with organic anions) is modelled as a gibbsite equilibrium:

$$[Al] = K_{Al} \cdot [H]^3 \quad (7)$$

and the bicarbonate concentration by the standard equilibrium equation:

$$[HCO_3] = K_{HCO_3} / [H] \quad (8)$$

with equilibrium constants K_{Al} and K_{HCO_3} . This shows that Ac_{le} can be expressed as a function of $[H]$ alone.

Expressing BC_{le} in eq.1 in terms of the other ions of the charge balance (eq.2) and using eqs.3-9, we can write the mass balance for base cations as:

$$CEC_a \cdot \frac{db}{dt} = -S_{dep}(t) - f_{net} \cdot N_{dep}(t) - Cl_{dep} + N_u + BC_{in} + Ac_{le}([H]) \quad (9)$$

where Ac_{le} as a function of $[H]$ is given by eqs.6-8. The time development of S_{dep} and N_{dep} determines the base saturation at any point in time since the deposition of base cations and chloride is assumed constant over time.

2.2 Empirical relationships between base saturation and pH

To “close” the above-described system of equations, we need a relationship between base saturation and the proton concentration $[H]$. In deterministic models of soil acidification, e.g. SMART (de Vries et al. 1989), the pH ($= -\log_{10}[H]$) is calculated from equations describing cation exchange, charge balance and mass balances for the individual ions. However, this involves solving a system of (non-linear) equations many times for a single site, which would require too many computer resources for use in optimisation calculations. Therefore we derive in the following an empirical relationship between base saturation and pH.

Both measurements and deterministic models suggest an S-shaped relationship between base saturation and pH. Therefore, Bloom and Grigal (1985) used the

following functional relationship between base saturation, b , and proton concentration, $[H]$:

$$pH = pH_{0.5} + a \cdot \log_{10} \left(\frac{b}{1-b} \right) \quad \text{or} \quad [H] = [H]_{0.5} \cdot \left(\frac{1-b}{b} \right)^a \quad (10)$$

with $pH_{0.5}$ is the pH at a base saturation of 0.5 (50%). They derived $pH_{0.5} = 4.96$ and $a = 0.797$ from measurements on 59 forested sites in the USA.

In earlier versions of the RAINS (Regional Acidification INFORMATION and Simulation) model for Europe (Alcamo et al. 1990), a simple dynamic soil acidification module was incorporated which described the base saturation – pH relationship as (Kauppi et al., 1986) according to:

$$pH = 4 + 1.6 \cdot b^{3/4} \quad (11)$$

This base saturation – pH curve was derived from results of an equilibrium model investigated by Reuss (1983).

Another approach has been used by Kaitala et al. (1992) who used the following differential equation relating base saturation directly to total deposition, $D(t)$:

$$\frac{db}{dt} = \alpha \cdot b - \beta \cdot b \cdot \log(b) - \gamma \cdot D(t) \cdot b \quad (12)$$

where α , β , γ are soil specific positive constants based on simulations with an ion-exchange model by Holmberg (1990).

The relationship in equation 10 has an infinite first derivative for $b=0$ and $b=1$ and equation 11 has an infinite first derivative for $b=0$, which makes them difficult to use in optimization models. Equation 12 only gives base saturation as a function of time but does not calculate soil solution chemistry. It thus cannot be linked to critical limit values for, e.g., pH or aluminium, which is crucial for evaluating effects of emission reductions. We therefore derived a new pH – base saturation relationship based on results of the model SMART. Simulations with SMART for a soil with different net acid inputs yielded the base saturation - pH relationships are depicted in Figure 1, showing the typical S-shape. These relationships depend only very weakly on soil parameters such as CEC or exchange and equilibrium constants, but do depend on the concentration of net acidity in the soil solution.

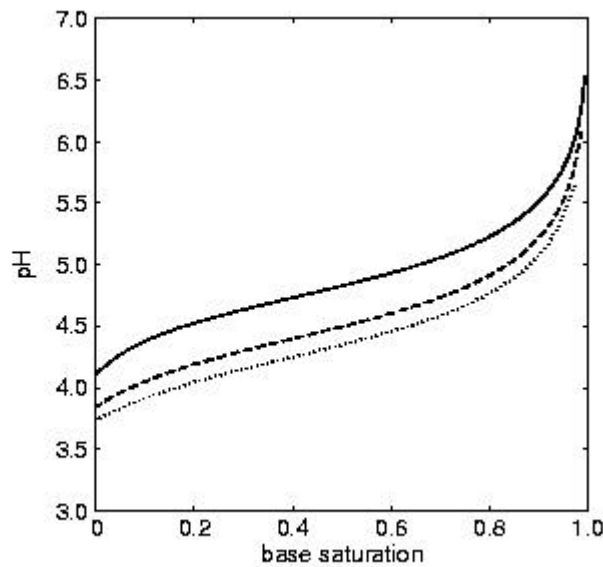


Figure 1 Relationship between base saturation and pH for a soil with $CEC_a = 32.5 \text{ eq.m}^{-2}\text{.yr}^{-1}$, initial base saturation of 100 %, net acid input of 10 (solid), 50(dashed) and 100 (dotted) $\text{eq.m}^{-2}\text{.yr}^{-1}$ and a precipitation surplus of 500 mm.yr^{-1} , as simulated with the SMART model

We used the following ninth-order polynomial describing the relationship between pH and base saturation, with an additional linear term accounting for the dependence on the net acidity input concentration (see also Figure 1):

$$pH = a_1 + a_2 \cdot (b - 0.5) + a_3 \cdot (b - 0.5)^9 - a_4 \cdot [Ac]_{net} \quad (13)$$

with:

a_1, a_2, a_3	dimensionless regression coefficients
a_4	regression coefficient ($\text{m}^3\text{.eq}^{-1}$)
$[Ac]_{net}$	concentration of net acidity input (eq.m^{-3}), the sum of S and N input minus base cation input divided by the precipitation surplus

The parameters a_1 to a_4 have been derived by non-linear regression from data sets with simulated base saturation, pH and net acidity concentration obtained by running the SMART model from its initial condition (in 1960) to 1992 on about 58000 forest soil combinations described in chapter 3. Regression analyses were carried out on four soil groups, characterised by their texture class, resulting in a set of 16 parameters characterising European forest soils (see Table 1).

Figure 2 shows the data sets and three base saturation – pH curves fitted to these data for $[Ac]_{net}$ equal to $-5, 0$ and $+5 \text{ eq.m}^{-3}$.

Table 1 Parameters a_1 to a_4 from the regression analyses for the 4 groups of texture classes

SoilGroup	a_1	a_2	a_3	a_4 ($\text{m}^3\cdot\text{eq}^{-1}$)
1 (texture 1)	5.100	0.939	465.9	0.246
2 (texture 2)	4.861	1.207	550.9	0.116
3 (texture 3+4+5)	4.828	0.981	692.6	0.0855
4 (peat)	5.054	1.084	728.1	0.0715

The ‘clouds’ of points in the last two graphs are caused by the method to initialise base saturation in 1960 (cf. de Vries et al., 1994) in combination with a slow changing base saturation due to the high CEC for these soil groups. Sensitivity tests showed that the parameters of the regression curves change only marginally if another end-year or other deposition scenarios are chosen.

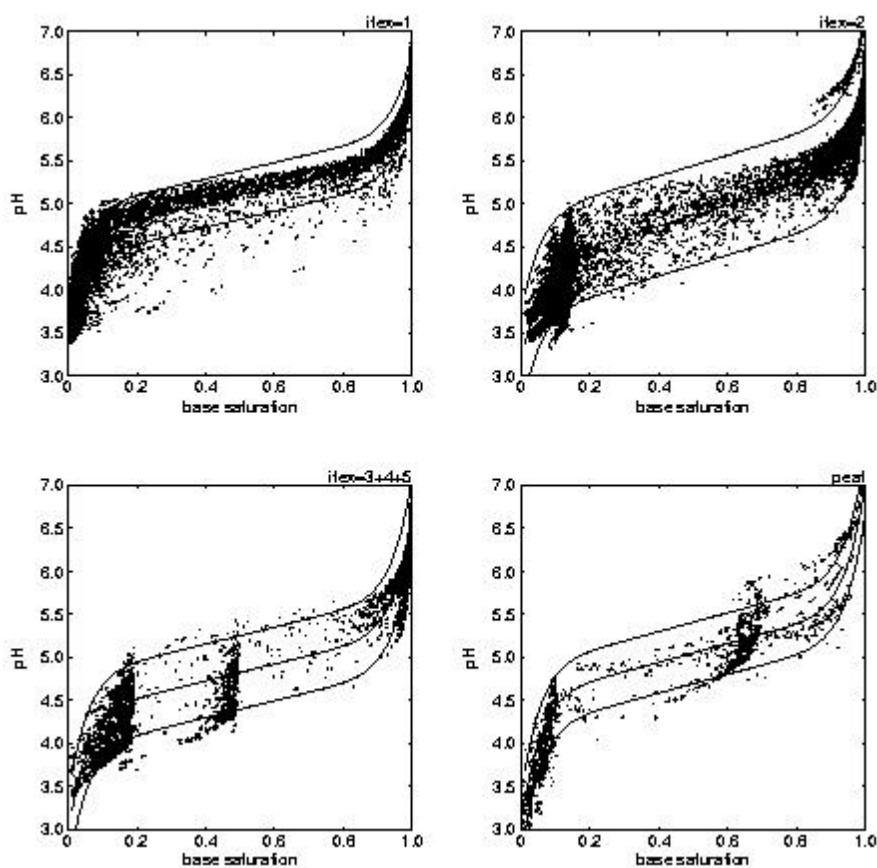


Figure 2 Data sets and fitted ninth-order polynomials (see eq. 13) for 4 soil groups and 3 levels of $[\text{Ac}]_{\text{net}}$ (-5 (upper curves), $=0$ (center curves) and $=+5$ (lower curves) $\text{eq}\cdot\text{m}^{-3}$)

2.3 Summary of model and input data required

The semi-empirical dynamic soil acidification model described in the previous section can be summarised as follows (see eq. 6-9 and 13):

$$CEC_a \cdot \frac{db}{dt} = -Ac_{net}(t) + Ac_{le} \quad (A)$$

with:

$$Ac_{net}(t) = S_{dep}(t) + f_{net} \cdot N_{dep}(t) - N_u - BC_{in} + Cl_{dep}$$

and

$$BC_{in} = BC_{dep} + BC_{we} - BC_u$$

$$Ac_{le} = Q \cdot ([H] + K_{Al} \cdot [H]^3 - K_{HCO_3} / [H]) \quad (B)$$

$$3 - \log_{10}[H] = pH = a_1 + a_2 \cdot (b - 0.5) + a_3 \cdot (b - 0.5)^9 - a_4 \cdot Ac_{net}(t) / Q \quad (C)$$

Equation A is solved for each time step (year) by inserting the base saturation from the previous time step into eq. C and using the resulting H-concentration to compute the acidity leaching via eq. B. Inserting this acidity leaching as well as the deposition of S and N into the right-hand side of eq. A yields the change in base saturation. The initial base saturation $b_0 = b(0)$, i.e. the base saturation at the starting year of the simulation, is taken from a SMART model run with historical depositions. The system of equations A-C not only gives the base saturation for every year; it also provides the concentration of aluminium and the pH, which are often used as indicators for soil acidification. Table 2 summarises the parameters needed in the model (note that f_{net} , N_u , BC_{in} and Cl_{dep} are model parameters and are assumed not to change over time):

Table 2 Parameters needed in the semi-empirical model

Parameter	Description	Values	Units	Dependent on
a_1, a_2, a_3	empirical parameters	see Table1	-	texture
a_4	empirical parameter	see Table1	$m^3 \cdot eq^{-1}$	texture
CEC_a	areal cation exchange capacity (= $? \cdot Z_r \cdot CEC$)	see Chap.3	$eq \cdot m^{-2}$	texture, grid
f_{net}	fraction of N_{dep} after correcting for denitrification and immobilisation	see Chap.3	-	texture, grid
Q	precipitation surplus	see Chap.3	$m \cdot yr^{-1}$	texture, grid
N_u	net uptake of nitrogen	see Chap.3	$eq \cdot m^{-2} \cdot yr^{-1}$	grid
BC_{in}	net input of base cations (deposition plus weathering minus net uptake)	see Chap.3	$eq \cdot m^{-2} \cdot yr^{-1}$	texture, grid
Cl_{dep}	deposition of chloride	see Chap.3	$eq \cdot m^{-2} \cdot yr^{-1}$	grid
K_{Al}	gibbsite equilibrium constant	300 3	$eq^{-2} \cdot m^6$ $eq^{-2} \cdot m^6$	for texture 1-5 for peat
K_{HCO_3}	= $pCO_2 \cdot KCO_2$		$(mol \cdot l^{-1})^2$	
KCO_2	dissociation constant of CO_2 (at 10°C)	0.0189	$(mol \cdot l^{-1})^2 \cdot atm^{-1}$	
pCO_2	partial pressure of CO_2 in soil	0.00948	atm	

3 Input data

3.1 Map overlays

Input data for the model presented in Chapter 2 include parameters describing cation exchange capacity, N transformation processes, precipitation surplus, nutrient uptake, and base cation weathering and -deposition. These input data vary as a function of location and receptor (the combination of forest type and soil type) as shown in Table 3.

Table 3 The influence of location, land use and soil type on input data

Input data	Location	Forest type	Soil type ¹⁾
Cation exchange capacity	-	-	x
N immobilisation	X	-	x
Dentrification	-	-	x
Precipitation surplus	X	x	x
Net N and BC uptake	X	x	(x)
Base cation weathering	X	-	x
Base cation deposition	X	x	-

¹⁾ Values in brackets imply that soil type may influence the input data, but it has not been accounted for in the data presented.

A receptor map with the required information to derive the input data for the model was constructed by overlaying the following maps:

- A map with EMEP grid cells of 150×150 km² (Saltbones and Dovland, 1986) that geo-references acid deposition and climate data estimates.
- A map with soil types at scale 1:1,000 000 for the countries within the EU and central Europe version 3 (Eurosoil, 1999) and the FAO 1:5,000,000 soil map for the Scandinavian countries, Russia, the Baltic states and former Yugoslavia (FAO, 1981).
- A map with forest types in Europe. This map was constructed using detailed NOAA-AVHRR satellite images (with a resolution of approximately 1×1 km²), and distinguishes conifers- broad-leaved- and mixed forest based on differences in their reflection (Mücher et al., 2000).
- A map with climate zones for Europe, derived from EC/UN-ECE (1996).
- A map with altitude zones in steps of 500 m, derived from detailed elevation data from the USGS (Row et al., 1995).

The resulting map contains about 83000 different forest-soil combinations; their allocation in EMEP grid cells is shown in Figure 3. Discarding units smaller than 1 km² reduces this number to 57240. In this application, the term forest soil refers to the combination of a tree species and a soil type. Regarding tree species, a distinction was made between coniferous and deciduous trees since data on the geographical distribution of various tree species (e.g. pine, fir, spruce, oak, beech and birch) could not be derived from the satellite images (Mücher et al., 2000).

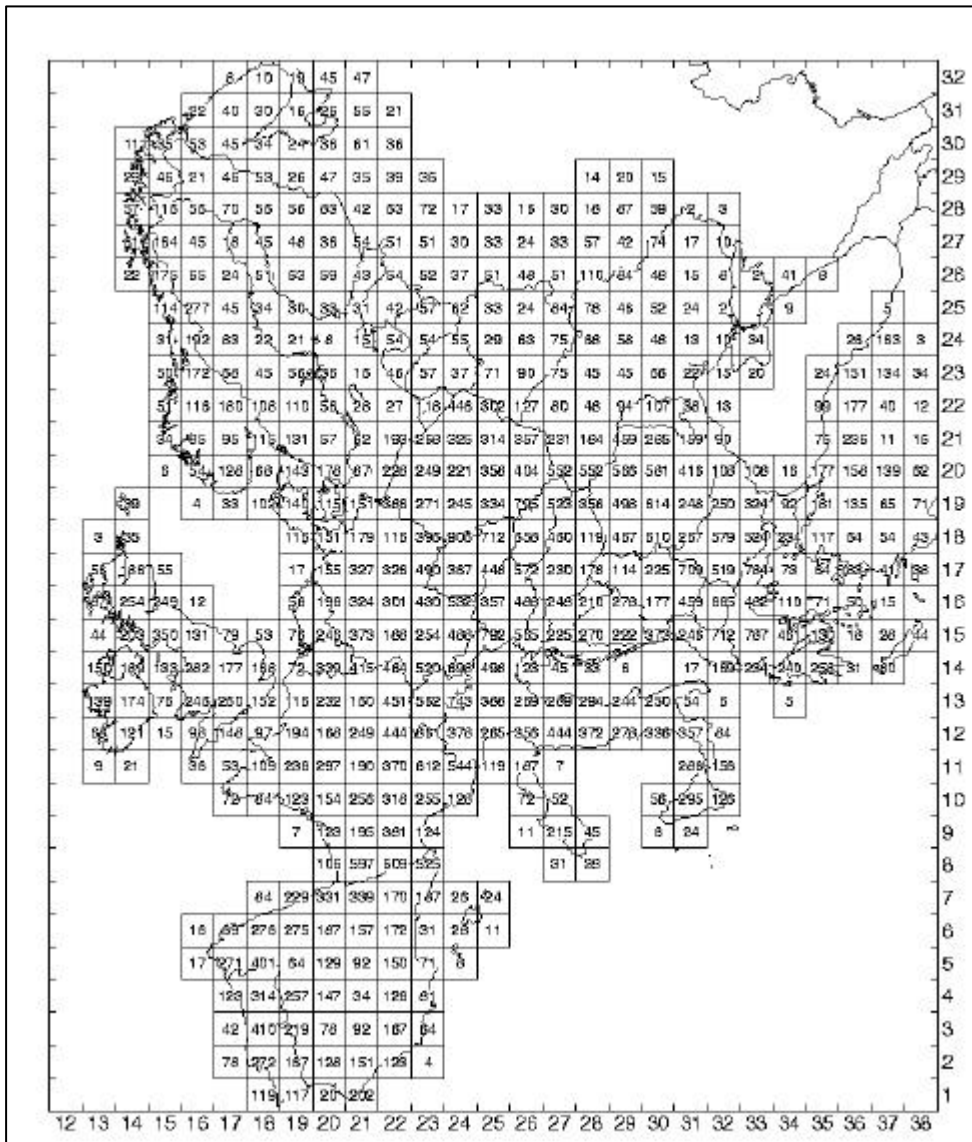


Figure 3. The number of computation units (forest soil combinations) for the EMEP 150 grid

Soil types were distinguished on the basis of the 1:1M and 1:5M soil maps of Europe. The soil map is composed of so-called soil associations, each polygon on the map representing one association. Every association, in turn, consists of several soil typological units (soil types) that each cover a known percentage of the soil association. The soil typological units on the map have been classified into more than 200 soil types, given in Annex 1.

For each soil typological unit information is available on e.g. soil texture and slope. Texture classes are defined in Table 4 (Eurosoil, 1999):

Table 4 Soil texture classes

Class	Name	Definition
1	Coarse	> 65 % sand and < 18 % clay
2	medium	> 15 % sand and < 35 % clay; > 18 % clay if sand > 65 %
3	medium fine	< 15 % sand and < 35 % clay
4	fine	> 35 % clay but < 60 % clay
5	very fine	> 60 % clay
9	organic soils	Soil types O

Table 5 gives the forested areas for each country derived from the forest map. This table shows that large differences exist in the percentage of forest per country. Lowest percentages are found in Ireland, Moldavia and the Netherlands (< 10 %), highest percentages occur in Austria, Estonia, Latvia, Sweden and Finland (> 50 %). The forested area in countries with many small lakes (e.g. Sweden and Finland) is overestimated due to the similar reflection of forest and lakes on the satellite images; in these countries some lakes have been classified as forested areas. For most countries, however, the forest area derived from the satellite data is in good accordance with the area given by forest statistics (Mücher et al., 2000).

Table 6 shows the distribution of forest over soil types in Europe for the 10 most common forest-soil types derived from the overlay of the soil- and forest map. Most forests are located on Podzols (Po, Pl, Pg, Ph together about 23%), especially in the Nordic countries, and to a lesser extent on Podzoluvisols (De, Dd, about 13%), Cambisols (Be, Bd and other Cambisols about 21 %), Luvisols (Lo, Lg, Lc about 9%) and Lithosols (I, about 4.3%). Forest soils occur mainly on coarse (texture class 1, 34 %) and medium textures (class 2, 58 %). Forests on medium fine (class 3, 4.6 %) and fine and very fine textures (classes 4 and 5, about 5%) are relatively rare. About 10% of European forests are located on peat soils (Od and Oe). Some inaccuracy in these estimates exists, because the soil map consists of soil associations. The map overlay thus gives a forested area for each association, not for each soil type. Forests have been assigned evenly to all soil types within the association, which in reality will not always be the case. However, an earlier study (De Vries et al., 1993) showed that when forest are assigned to poor soils in an association first (instead of evenly distributed), this hardly makes a difference in the forested area per soil type on a European scale.

Table 5. Forested areas in Europe

Country	Area				Country	% Forest
	Conifers	Mixed	Deciduous	Total forest		
AL	6326	2141	1935	10402	28750	36
AT	28707	18456	5252	52415	83845	63
BA	3143	8673	18176	29993	51233	59
BE	785	1989	3172	5946	30518	19
BG	11301	8767	22866	42933	110994	39
BY	60990	19017	7005	87012	207595	42
CH	7521	6881	5099	19501	41285	47
CZ	13955	8256	3054	25264	78864	32
DE	46132	31019	28877	106029	357022	30
DK	898	1274	3319	5491	43094	13
EE	8687	10877	10226	29790	45227	66
ES	67025	19290	14546	100862	497509	20
FI	217528	26744	13695	257968	338144	76
FR	40449	28595	55745	124789	543965	23
GB	10217	6966	6268	23452	241752	10
GR	22782	4464	5611	32856	131957	25
HR	2879	2757	10755	16391	56538	29
HU	2585	3251	5048	10884	93030	12
IE	1656	1385	1413	4455	70285	6
IT	31602	25673	38936	96211	301302	32
LT	13386	3919	1656	18962	65200	29
LU	30	303	421	753	2586	29
LV	15147	12991	7806	35945	64100	56
MD	988	477	825	2291	33700	7
MK	2331	2659	7259	12249	25713	48
NL	1657	327	70	2054	41865	5
NO	105415	13036	3712	122163	323877	38
PL	69267	17591	8402	95260	312685	30
PT	6533	6366	3626	16524	92391	18
RO	20072	19973	50240	90285	237499	38
RU ¹⁾	237898	86399	116833	441131		
SE	304383	27045	7277	338705	449964	75
SI	2482	4791	6383	13656	20273	67
SK	6978	6258	11588	24824	49036	51
TR ¹⁾	29666	6997	18210	54872		
UA	54464	19759	16732	90954	603700	15
YU	6522	10567	24488	41576	88412	47
Europe	1462388	475934	546526	2484847		

¹⁾ Part within modeling domain

Table 6 Area of the 10 most common forest-soil combinations in Europe

Soil Type	Area (km ²)	% area
Po	453891.6	17.0
De	321712.6	12.1
Bd	253857.3	9.5
Od	236342.8	8.9
Be	121030.9	4.5
I	114681.1	4.3
Lo	76836.03	2.9
Lg	75044.08	2.8
E	72605.32	2.7
Pl	56493.99	2.1

3.2 Input data for the model

The model described in Chapter 2 needs the following input parameters (see Table 2):

- Cation exchange capacity (CEC_a)
- Base cation weathering (BC_{wb})
- Immobilisation and denitrification (f_{ned})
- Net growth uptake of N and BC (N_u and BC_u)
- Precipitation surplus (Q)
- Deposition of base cations and chloride (BC_{dep} and Cl_{dep})

Cation exchange capacity

In the model the cation exchange capacity is needed per unit area (eq.m²). This parameter was obtained by:

$$CEC_a = r \cdot Z_r \cdot CEC \quad (14)$$

with:

? bulk density (g.cm⁻³)

Z_r soil depth (m)

CEC cation exchange capacity (meq.kg⁻¹)

While Z_r was set to 0.5 m for all forest soils (except for lithosols where Z_r is set to 0.1 m), ? was computed from organic C content and clay content by the following transfer functions (Hoekstra and Poelman, 1982; Wallenburg, 1988):

$$r = \begin{cases} 1/(0.625 + 0.05 \cdot ctC + 0.0015 \cdot clay) & \text{for } ctC < 5\% \\ 1.55 - 0.0814 \cdot ctC & \text{for } 5\% \leq ctC \leq 15\% \\ 0.725 - 0.337 \cdot \log_{10} ctC & \text{for } ctC > 15\% \end{cases} \quad (15)$$

Where ctC and $clay$ are the organic carbon content and clay content in percent, respectively. For ctC between 5 and 15% the given equation is a linear interpolation between the other two equations (for $clay=0$). For CEC the following transfer function by Breeuwsma et al. (1986) is used:

$$CEC = 5 \cdot clay + 27.25 \cdot ctC \quad (16)$$

Clay content is an attribute to the soil map (see above); for the soil map five texture classes are defined, each with a range in clay, sand and silt content. The average clay content in the class was used to characterise the soil. Organic carbon content for each soil type was derived from European wide databases (de Vries et al., 1993; Vanmechelen et al., 1997).

Base cation weathering

Weathering of base cations was computed as a function of parent material class and texture class and corrected for temperature, as described by De Vries et al. (1993). Parent material classes were assigned to soil types according to Table 7.

Table 7 Conversion between soil type and parent material class

Parent material	FAO soil type
Organic	O, Od, Oe, Ox
Acidic	Ah, Ao, B, Bd, Be, Bh, D, Dd, De, Dg, Gx, I, Jd, P, Pg, Ph, Pl, Po, Pp, Q, Qc, Ql, Rd, Rx, U, Wd
Intermediate	Af, Bv, C, Cg, Ch, Cl, G, Gd, Ge, Gh, Gm, H, Hg, Hh, Hl, J, Je, Jt, Kh, L, La, Lf, Lg, Lo, Mo, R, Re, V, Vp, W, We
Basic	F, T, Th, Tm, To, Tv
Calcareous	Bc, Bg, Bk, Ck, E, Gc, Hc, Jc, K, Kk, Kl, Lc, Lv, Rc, S, Sg, Sm, So, Vc, X, Xh, Xk, Xl, Xy, Zg, Zm, Zo

Acidic : Sand (stone), gravel, granite, quartzine, gneiss (schist, shale, greywacke, glacial till)

Intermediate : Gronodiorite, loess, fluvial and marine sediment (schist, shale, greywacke, glacial till)

Basic: Gabbro, basalt, dolomite, volcanic depositis.

Weathering rate classes are given in Table 8 as a function of texture class (Table 4) and parent material class (Table 7).

The actual weathering rate for non-calcareous soils was then computed according to:

$$BC_{we} = 0.05 \cdot (WRc - 0.5) \cdot Z_r \cdot \exp\left(\frac{A}{(273 + T_{avg})} - \frac{A}{(273 + T)}\right) \quad (17)$$

with:

BC_{we} base cation weathering rate ($\text{eq.m}^{-2}.\text{yr}^{-1}$)

WRc weathering rate class

A pre-exponential factor of 3600 K (Sverdrup, 1990)

T_{avg} average temperature for soil with weathering rate class WRc ($^{\circ}\text{C}$)

T actual (soil) temperature ($^{\circ}\text{C}$)

Table 8 Weathering rate classes as a function of texture and parent material

Parent Material	Texture class				
	1	2	3	4	5
Acidic	1	3	3	6	6
Intermediate	2	4	4	6	6
Basic	2	5	5	6	6
Organic	class 6 for Oe and class 1 for other organic soils				

Without temperature correction this means that weathering rates vary from 0.025 eq.m⁻².yr⁻¹ for class 1 to 0.275 eq.m⁻².yr⁻¹ for class 6 for a soil of 1m depth. The average temperature for each weathering rate class was computed by averaging mean yearly temperatures for each computation unit on the soil map with that specific weathering rate class.

Weathering rate fractions of Ca, Mg, K and Na were estimated as a function of clay and silt content (in %) for texture classes 2 to 5 (Van der Salm, 1999) and as fixed fractions of total weathering for texture class 1 (De Vries, 1994) according to the following equations:

$$XCa = \begin{cases} 0.3 & \text{for texture class 1} \\ 1.6 \cdot \text{clay} - 19.5 & \text{for texture class 2,4,5} \\ 0.34 \cdot \text{clay} + 0.07 \cdot \text{silt} - 6.19 & \text{for texture class 3} \end{cases} \quad (18a)$$

$$XMg = \begin{cases} 0.3 & \text{for texture class 1} \\ 0.70 \cdot \text{clay} - 7.0 & \text{for texture class 2,4,5} \\ 0.08 \cdot \text{clay} - 0.17 & \text{for texture class 3} \end{cases} \quad (18b)$$

$$XK = \begin{cases} 0.2 & \text{for texture class 1} \\ 0.06 \cdot \text{clay} - 0.43 & \text{for texture class 2,4,5} \\ 0.032 \cdot \text{clay} + 0.037 \cdot \text{silt} - 2.18 & \text{for texture class 3} \end{cases} \quad (18c)$$

$$XNa = \begin{cases} 0.2 & \text{for texture class 1} \\ 0.05 \cdot \text{clay} + 0.2 & \text{for texture class 2,4,5} \\ 0.036 \cdot \text{silt} - 1.55 & \text{for texture class 3} \end{cases} \quad (18d)$$

These fractions were then normalized, e.g. $xCa = XCa / (XCa + XMg + XK + XNa)$, resulting in $xCa + xMg + xK + xNa = 1$.

Denitrification and immobilisation

Immobilisation and denitrification were modelled by the fraction f_{net} , which is computed as:

$$f_{net} = (1 - f_{de}) \cdot (1 - f_{imm}) \quad (19)$$

The denitrification fraction, f_{de} , was computed as a function of drainage status, which is known for each soil on the soil map:

Table 9. Relation between drainage status and denitrification fraction

Drainage	Excessive	Well	Mod. Well	Imperfect	Poor	Very Poor
f_{de}	0.0	0.1	0.2	0.4	0.7	0.8

The immobilisation fraction, f_{imm} , was computed from the C/N ratio of the soil, which was estimated from the N deposition in the starting year and the known organic matter content of the soil (de Vries et al., 1994).

Nutrient uptake

Net uptake of base cations, BC_u , and nitrogen, N_u , was computed by multiplying the estimated growth of stems and branches with the element contents of BC and N in these compartments.

Forest growth was estimated as a function of climate zone, forest type, altitude zone and stand quality according to the procedure described by Klap et al. (1997). In this procedure, a site quality is computed which is combined with yield tables that give forest growth as a function of forest type, forest age and climate zone (combination of climate and altitude; Klap et al., 1997) for each site quality.

Site quality was estimated from drainage status, fertility status (expressed by the C/N ratio in the soil) and available water content in combination with precipitation deficit, corrected for soil acidity. Values for drainage status and available water content (each subdivided in 7 classes) are provided in the database associated to the soil map. Annex 2 gives an overview of the classifications used to derived site quality. Forest types were derived from the forest map (see section 3.1); mixed forests were treated as conifers forests. Since forest age is not known, the average growth of a rotation period from the yield table was used (see Annex 3).

Data for element contents in stems and branches were computed according to (see De Vries et al., 1993):

$$ctX = ctX_{\min} + a (ctX_{\max} - ctX_{\min}) \quad 0 \leq a \leq 1 \quad (20)$$

where ctX_{\min} and ctX_{\max} are the minimum and maximum contents (eq.kg⁻¹) of element X in stems or branches and a is a latitude dependent factor, based on data for boreal forests given in Rosén (1990).

For X = N, Mg and K, a was set equal to:

$$a = \begin{cases} 1 & \text{for } latitude \leq 55^\circ \\ (65^\circ - latitude) / 10^\circ & \text{for } 55^\circ < latitude < 65^\circ \\ 0 & \text{for } latitude \geq 65^\circ \end{cases} \quad (21)$$

And for X=Ca, a is set equal to:

$$\mathbf{a} = \begin{cases} 0 & \text{for } latitude \leq 55^\circ \\ (latitude - 55^\circ) / 10^\circ & \text{for } 55^\circ < latitude < 65^\circ \\ 1 & \text{for } latitude \geq 65^\circ \end{cases} \quad (22)$$

Using these equations, element contents in stems and branches of boreal forests (above latitude 55°) are either lower (N, Mg and K) or higher (Ca) than in central and southern European forests (below latitude 55°). Values for the minimum and maximum element contents are given in Table 10.

Table 10 Minimum and maximum values of nitrogen and base cation contents in stems and branches of coniferous and deciduous forests in Europe

Forest type	Compartment	Minimum contents				Maximum contents			
		N	Ca	Mg	K	N	Ca	Mg	K
Conifers	Stems	0.10	0.08	0.02	0.05	0.10	0.16	0.02	0.05
	Branches	0.20	0.30	0.03	0.10	0.40	0.60	0.05	0.25
Deciduous	Stems	0.15	0.13	0.04	0.10	0.15	0.21	0.04	0.10
	Branches	0.20	0.45	0.03	0.05	0.40	0.75	0.05	0.20

Base cation and chloride deposition

The bulk deposition (wet deposition and a very small part of dry deposition) of base cations and chloride was derived from 89 to 96 (depending on the ion) EMEP/CCC monitoring stations in Europe (Hjellbrekke et al., 1998) averaged over the years 1991-1995. Grid values were derived by interpolating between the $n=5$ nearest stations according to:

$$X_{dw,i} = \sum_{j=1}^n \frac{X_{dw,j}}{r_{i,j}} \bigg/ \sum_{j=1}^n \frac{1}{r_{i,j}} \quad \text{with } X = Ca, Mg, K, Na, Cl \quad (23)$$

where $X_{dw,i}$ and $X_{dw,j}$ are the wet (bulk) deposition of ion X in grid i and at station j respectively and $r_{i,j}$ is the distance of the center of grid i to station j . The sea-salt corrected wet base cation deposition, BC_{dw}^* , is computed by assuming that all chloride originates from sea-salt. (Posch and de Vries, 1999).

The influence of dry deposition on the total deposition has been accounted for by multiplying the wet (bulk) deposition according to:

$$BC_{dep}^* = (1 + f_{dd}) \cdot BC_{dw}^* \quad (24)$$

where f_{dd} is a dry deposition factor. The value of f_{dd} was derived from the ratio of Na in bulk deposition and throughfall (Ulrich and Matzner, 1983; Bredemeier, 1988):

$$f_{dd} = (Na_{tf} - Na_{dw}) / Na_{dw} \quad (25)$$

Results of a literature survey by Ivens (1990) for 47 sites in Europe gave median values for f_{dd} of 0.6 for deciduous forests and 1.1 for coniferous forests. However,

these data were based on results in areas that are sparsely occupied by forests. It is to be expected that the dry deposition factor f_{dd} will decrease with an increase in the forested area within a grid. For the application on Europe, this effect was accounted for by a linear relationship between f_{dd} and the fraction of open land in the grid, f_o , according to:

$$f_{dd} = \beta \cdot f_o \quad (26)$$

where $\beta = 0.6$ for deciduous forests and $\beta = 1.1$ for coniferous forests.

Precipitation surplus

To compute the concentration and leaching of compounds in the soil, the annual water fluxes through the soil must be known. These water fluxes were derived from meteorological data available for the 0.5° longitude \times 0.5° latitude grid described by Leemans and Cramer (1991), who interpolated selected records of monthly meteorological data from 1678 European meteorological stations for the period 1931-1960.

Actual evapotranspiration was calculated according to a model used in the IMAGE global change model (Leemans and van den Born, 1994) following the approach by Prentice et al. (1993). Potential evapotranspiration is computed from temperature, sunshine and latitude. Actual evapotranspiration is computed using a reduction function for potential evapotranspiration based on the available water content in the soil described by Federer (1982). Soil water content is in turn estimated using a simple bucket-like model that uses water holding capacity (derived from the available soil texture data) and precipitation data. A full derivation of the model is given in Annex 4.

Precipitation surplus was computed as precipitation minus evapotranspiration minus interception evaporation. The latter term was computed according to (c.f. De Vries et al., 1993) :

$$I = g \cdot P^{0.75} \quad (27)$$

with:

P precipitation
 γ empirical factor

Values used for γ were 1.75 for conifers forest and 1.0 for deciduous forest based on Mitscherlich and Moll (1970) and Van Grinsven et al. (1987), respectively.

Input data on the EMEP 150-km grid

The input parameters for the application of the model (listed in Table 2) within the optimisation framework are derived by computing (area-weighted) average values per EMEP grid cell for each combination of the 4 soil groups (see Table 1) and 5 texture classes (1, 2, 3, 4+5 and organic soils). This results in 1366 computation units over Europe; their allocation to EMEP grid cells is shown in Figure 4.

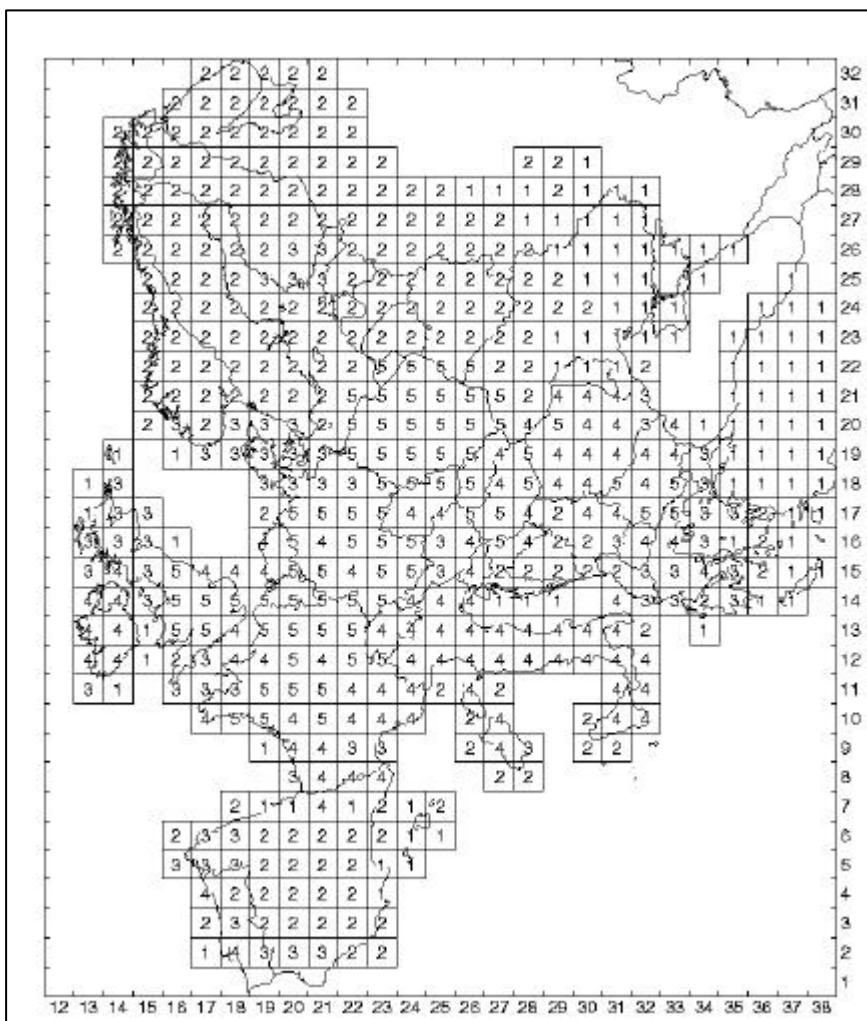


Figure 4. Number of aggregated computation units per EMEP 150 grid cell used in the optimisation model.

Figure 5 show the area-weighted values for the model's input parameters for each EMEP grid cell. Figure 5a show that the value of $f_{net} = (1-f_{d}) \cdot (1-f_{imm})$ is highest in areas with a high N deposition where N immobilization is low because of N saturated soils (soils with a low C/N ratio). CEC values (expressed on an areal basis) vary between $<60 \text{ eq.m}^{-2}$ in areas dominated by poor sandy soil to about 120 eq.m^{-2} in areas with rich (e.g. loess) soils. Figure 5c shows the sum of the base cation input by deposition and weathering and N removal by uptake as an indicator for acid input buffering. This figure shows that high values for this parameter occur in areas with high base cation deposition (southern Europe) and in areas with soils that have a high base cation weathering rate (compare Figure 5b). Figure 5d shows the precipitation surplus over Europe. High values ($> 600 \text{ mm.yr}^{-1}$) are found in high rainfall areas such as the UK and Ireland, north-western Spain, southern Norway and the alpine region; lowest values ($< 150 \text{ mm.yr}^{-1}$) are found in e.g. central Europe and central Spain.

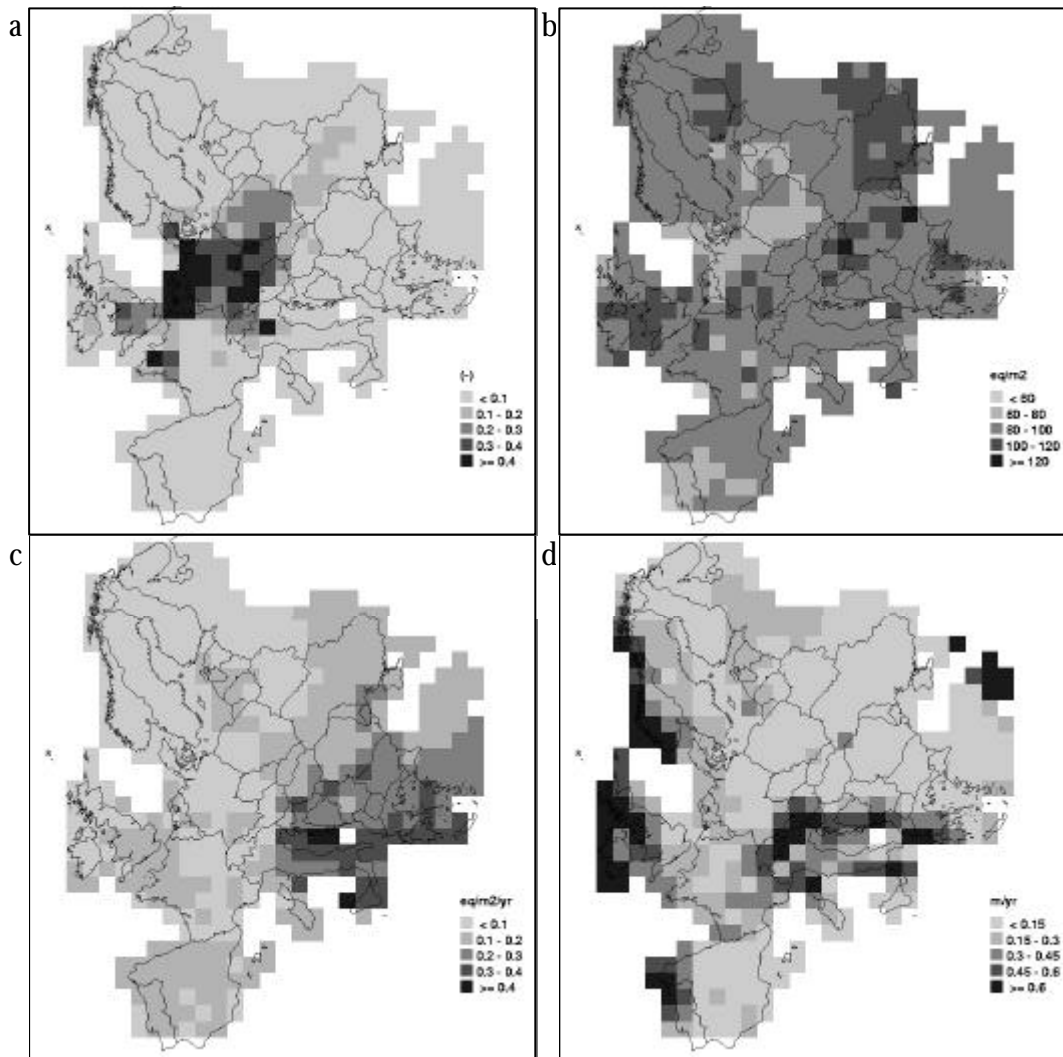


Figure 5 Area weighted average parameters values for each EMEP grid cell for the model input parameters (a) f_{net} , (b) CEC_a , (c) $BC_{in} + f_{net} \cdot N_u$, (d) and Q .

4 Model results

To test the performance of the model, simulation results for Europe (using the full set of about 100000 computation units on the 0.5° longitude \times 0.5° latitude grid) were compared with simulation results from SMART using the same initial conditions and deposition-scenario (transition to protocol deposition in 2010 and constant deposition thereafter). Maps of the simulated aluminium concentration in 2060 from both models are shown in Figure 6.

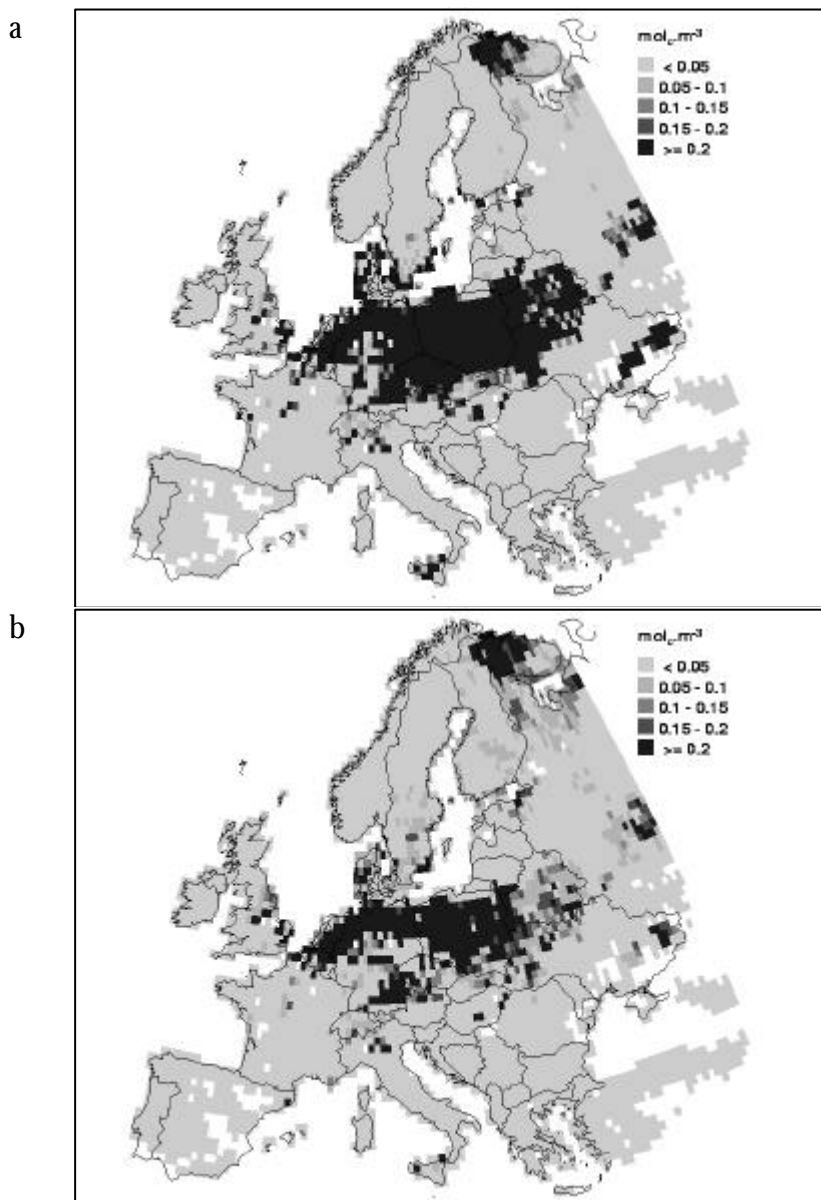


Figure 6. Simulated Al concentration in 2060 with (a) SMART and (b) the semi-empirical model

Results show that the semi-empirical model gives similar results as SMART for large parts of Europe but underestimates acidification in central Europe (south eastern part of Germany and the north part of the Czech Republic, compare measurements given by Vanmechelen et al., 1997). This is most likely due to the initialisation of the model: the initial base saturation is computed in equilibrium with the 1960 deposition. In these regions with a high initial acid input, a relatively high base saturation is computed in the beginning of the simulation period because the pH – base saturation relationship (see Figure 2) is dependent on acid input and fairly flat for intermediate values (0.2 and 0.8), so a low pH value (from acid input) can be connected to a high base saturation level. This effect on a regional scale is shown in Figure 7. This figure shows the overestimation of the base saturation in the southeastern part of Germany and the north of the Czech republic.

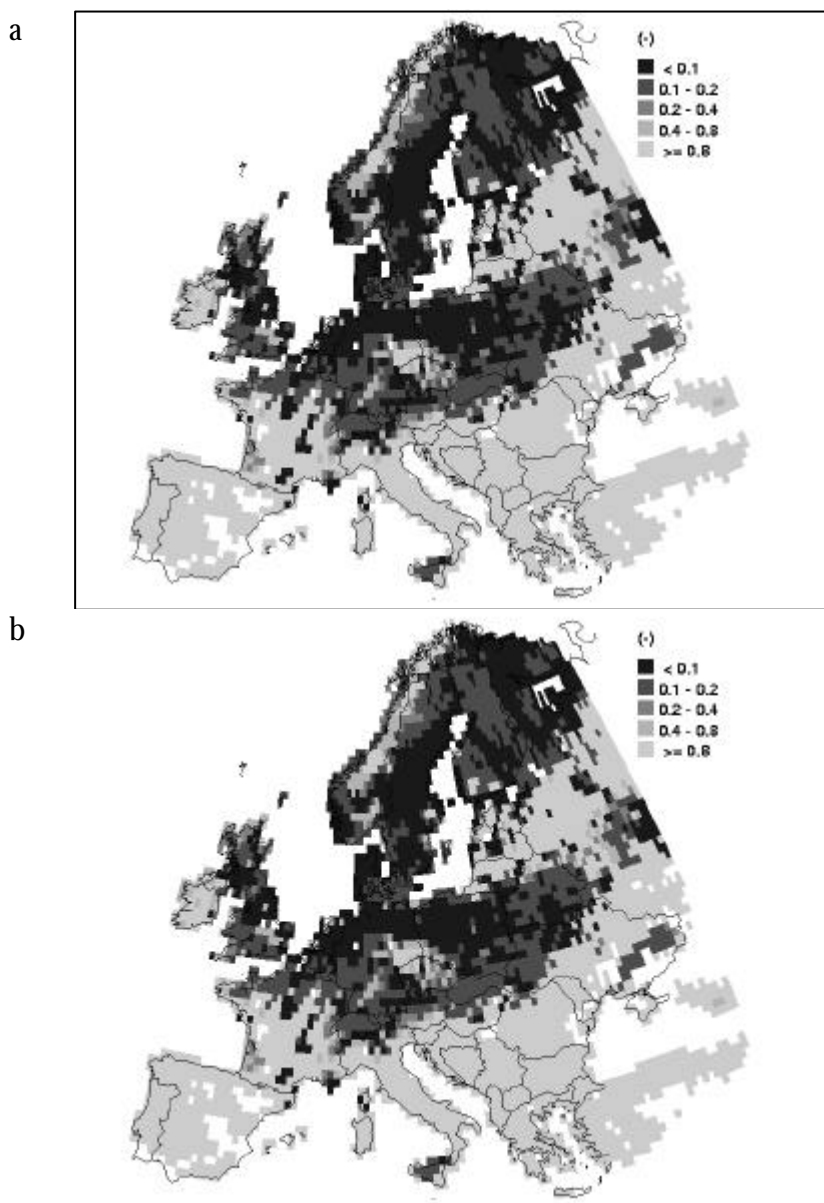


Figure 7. Simulated base saturation in 1990 with (a) SMART and (b) the semi-empirical model

This figure also shows that the base saturation in 1990 in most regions in Scandinavia computed with the semi-empirical model is lower than that computed with SMART.

Figure 8 shows the cumulative frequency distributions of the simulated $[Al^{3+}]$ in the soil solution for both models in 1990 and 2060.

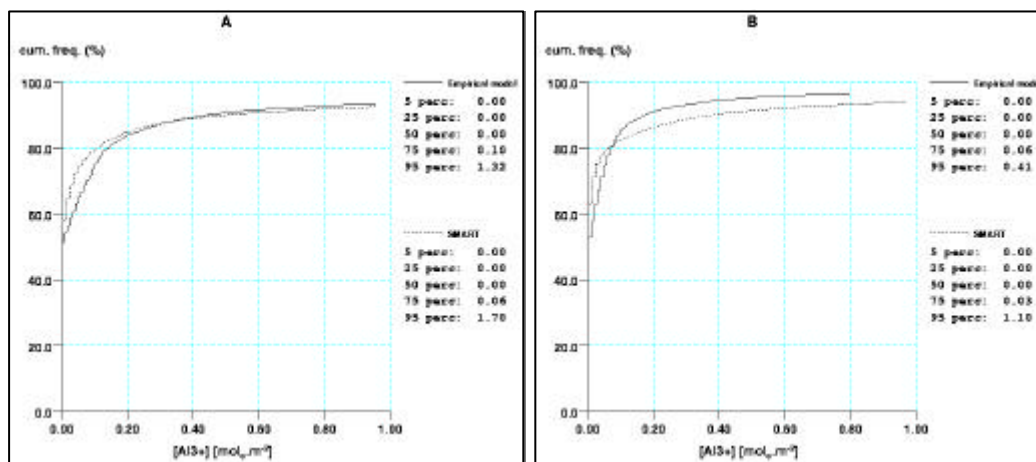


Figure 8. Cumulative frequency distributions of the simulated $[Al^{3+}]$ in the soil solution for both models in (a) 1990 and (b) 2060

This figure shows that the area with an aluminum concentration above $0.2 \text{ eq} \cdot \text{m}^{-3}$ (the critical limit) is about equal for both models in 1990, whereas the area with an aluminum concentration above $0.2 \text{ eq} \cdot \text{m}^{-3}$ in 2060 is higher for SMART than for the semi-empirical model. This indicates that the semi-empirical model simulates a faster recovery from acidification than SMART.

5 Discussion and conclusions

A semi-empirical soil acidification model was derived that relates changes in base saturation to input of acid and base cation deposition through a relationship with pH. The model consists of only three equations and computes, besides base saturation, the pH and aluminium concentration in the soil solution, which makes it suitable to be incorporated in integrated assessment models that aim at optimising emission abatement (both in space and time) using a maximum aluminium concentration (or a minimum pH) as a limiting condition.

The relationship between pH and base saturation was derived from numerous runs with the model SMART. Clear relationships were found for texture classes 1 and 2 (coarse and medium texture), whereas relationships for (heavy) clay soils and peat soils are less distinct. On a European scale, forest soils are dominantly coarse or medium textured soils (about 80 % of the total forested area) which means that for the majority of the soils a sound relationship between pH and base saturation could be derived.

A map with computation units was constructed by overlaying maps with soil, land-use, climate and altitude information. Especially the new soil- and forest map can be considered a major improvement compared to maps used in previous studies on the European scale (e.g., de Vries et al., 1994) as they contain more detailed and extensive information. A data set for the optimisation model was constructed by aggregating input data for the semi-empirical model for each EMEP 150-km grid cell. This reduces the number of computation units to about 1400.

The semi-empirical model was tested by comparing its results on a European scale with the results from SMART. Results show that some differences exist between the outcome of the models, and that on a European scale the semi-empirical model simulates a faster recovery from acidification than SMART at the same acid input. It therefore might give reasonable results for short simulation periods, but might give strongly deviating results for longer time periods. In some areas with a high initial acid input, high base saturation is computed by the semi-empirical model which is not in line with observations (Vanmechelen et al., 1997).

Instead of finetuning the semi-empirical model, future developments will concentrate on simplifying SMART into a very simple process-based dynamic soil acidification model since first tests show that it hardly increases the computational burden and gives results that are almost identical to the SMART model.

References

- Alcamo, J., R. Shaw and L. Hordijk (eds.), 1990. The RAINS model of acidification—Science and strategies in Europe. Kluwer Academic Publishers, Dordrecht, The Netherlands, 402 pp.
- Bloom, P.R. and D.F. Grigal, 1985. Modeling soil response to acidic deposition in nonsulfate adsorbing soils. *J. Environ. Qual.* 14(4):489-495.
- Bredemeier, M., 1988. Forest canopy transformation of atmospheric deposition. *Water, Air, and Soil Pollution* 40: 121-138.
- Breeuwsma, A., J.H.M. Wösten, J.J. Vleeshouwer, A.M. Van Slobbe and J. Bouma, 1986. Derivation of land qualities to assess environmental problems from soil surveys. *Soil Sci. Soc. Am. J.* 50: 186-190.
- De Vries, W., M. Posch and J. Kämäri, 1989. Simulation of the long-term soil response to acid deposition in various buffer ranges. *Water, Air and Soil Pollution* 48:349-390.
- De Vries, W., M. Posch, G.J. Reinds and J. Kämäri, 1993. Critical loads and their exceedance on forest soils in Europe. Report 58 (revised version), The Winand Staring Centre for Integrated Land, Soil and Water Research. Wageningen, The Netherlands.
- De Vries, W., G.J. Reinds, M. Posch and J. Kämäri, 1994. Simulation of soil response to acidic deposition scenarios in Europe. *Water, Air and Soil Pollution* 78:215-246.
- De Vries, W., 1994. Soil response to acid deposition at different regional scales. Ph.D. thesis, Agricultural University Wageningen, The Netherlands, 487 pp.
- EC/UN-ECE, 1996. Forest condition in Europe. EC-UN/ECE Brussels, Geneva, 1996, 128pp + Annexes.
- Eurosoil, 1999. Metadata: soil geographical data base of Europe v. 3.2.8.0. Eurosoil, Ispra, Italy.
- FAO, 1981. FAO-Unesco soil map of the world, 1:5.000.000; volume V Europe, Unesco-Paris, 199 pp.
- Federer, C.A., 1982. Transpirational supply and demand: Plant, soil, and atmospheric effects evaluated by simulation. *Water Resources Research* 18(2):355-362.

Hjellbrekke A.G., J. Schaug, J.E. Hanssen and J.E. Skjelmoen, 1997. Data report 1995. Part 1: Annual summaries. NILU CCC Report 4/97. Norwegian Institute for Air Research, Kjeller, Norway.

Hoekstra, C. and J.N.B. Poelman, 1982. Dichtheid van gronden gemeten aan de meest voorkomende bodemeenheden in Nederland. Wageningen, The Netherlands, Stichting voor Bodemkartering, Rapport nr. 1582. (In Dutch.)

Holmberg, M. 1990. Ion exchange dynamics and soil acidification: Model development and testing. Licentiate thesis, Helsinki University of Technology, Espoo, Finland.

Ivens, W. 1990. Atmospheric deposition onto forests. PhD thesis, University of Utrecht, The Netherlands, 153pp.

Jarvis, P.G., and K.G. McNaughton, 1986. Stomatal control of transpiration: Scaling up from leaf to region. *Advances in Ecological Research* 15:1-49.

Kaitala, V., M. Pohjola, and O. Tahvonen, 1992. Transboundary air pollution and soil acidification: A dynamic analysis of an acid rain game between Finland and the USSR. *Environmental and Resource Economics* 2:161-181.

Kauppi, P., J. Kämäri, M. Posch, L. Kauppi and E. Matzner, 1986. Acidification of forest soils: Model development and application for analyzing impacts of acidic deposition in Europe. *Ecological Modelling* 33:231-253.

Klap, J. W. de Vries, J.W. Erisman and E.P van Leeuwen, 1997. Relationships between forest condition and natural and anthropogenic stress factors on the European scale; pilot study. SC Report 150, The Winand Staring Centre for Integrated Land, Soil and Water Research. Wageningen, The Netherlands, 245 pp.

Leemans, R.. and W. Cramer, 1991. The IIASA database for mean monthly values of temperature, precipitation and sunshine on a global terrestrial grid. IIASA Research Report RR-91-18, International Institute of Applied System Analysis, Laxenburg, Austria, 61 pp.

Leemans, R.. and G.J. van den Born, 1994. Determining the potential distribution of vegetation, crops and agricultural productivity. *Water, Air and Soil Pollution* 76:133-161.

Linacre, E.T., 1968. Estimating the net-radiation flux. *Agricultural Meteorology* 5(1):49-63.

Mitscherlich, G. and W. Moll, 1970. Untersuchungen über die Niederschlags- und Bodenfeuchtigkeitsverhältnisse in einigen Nadel- und Laubholzbeständen in der Nähe von Freiburg. *A.F.J.Z.* 141 (3): 49-60

Mücher, S., K. Steinnocher, J.-L. Champeaux, S. Griguolo, K. Wester, C. Heunks and V. van Katwijk, 2000. Establishment of a 1-km pan-european land cover database for environmental monitoring. *International Archives of Photogrammetry and Remote Sensing*, Vol. XXXIII, Part B4, Amsterdam, pp. 702-709.

Posch, M., G.J. Reinds and W. de Vries, 1993. SMART – A Simulation Model for Acidification's Regional Trends: Model description and user manual. Mimeograph Series of the National Board of Waters and the Environment 477, Helsinki, Finland, 43 pp.

Posch, M. and W. de Vries, 1999. Derivation of critical loads by steady-state and dynamic soil models. In: S.J. Langan (Ed.): *The impact of nitrogen deposition on natural and semi-natural ecosystems*. Kluwer Academic Publishers, Dordrecht, Netherlands, pp. 213-234.

Prentice, I.C., M.T. Sykes and W. Cramer, 1993. A simulation model for the transient effects of climate change on forest landscapes. *Ecological Modelling* 65:51-70.

Priestley, C.H.B. and R.J. Taylor, 1972. On the assessment of surface heat flux and evaporation using large scale parameters. *Monthly Weather Review* 100:81-92.

Reuss, J.O., 1983. Implications of the calcium-aluminum exchange system for the effect of acid precipitation on soils. *J. Environ. Qual.* 12(4):591-595.

Rosén, K. 1990. *The critical load of nitrogen to Swedish forest ecosystems*. Uppsala, Sweden., Department of Forest Soils, Swedish University of Agricultural Sciences, 15 pp.

Row, L.W., D.A. Hastings and P.K. Dunbar, 1995. *TerrainBase Worldwide Digital Terrain Data - Documentation Manual*, CD-ROM Release 1.0. National Geophysical Data Center, Boulder, Colorado.

Salbones, J. and H. Dovland, 1986. *Emissions of sulphur dioxide in Europe in 1980 and 1983*. EMEP/CCC Report 1/86, Norwegian Institute for Air Research, Lillestrøm, Norway.

Schmieman, E.C. and E.C. van Ierland, 1999. Dynamics in soil acidification: an economic analysis. *Ecological Economics* 31: 449-462.

Schmieman, E., W. de Vries, L. Hordijk, C. Kroeze, M. Posch, G.J. Reinds and E. van Ierland, 2000. *Dynamic cost-effective reduction strategies for acidification in Europe: an application to Ireland and the United Kingdom*. (draft).

Sverdrup, H.U. 1990. *The kinetics of base cation release due to chemical weathering*. Lund University Press, Sweden, 246 pp.

Ulrich, B. and E. Matzner, 1983. Abiotische Folgewirkungen der weiträumigen Ausbreitung von Luftverunreinigung. Umweltforschungsplan der Bundesministers der Innern. Forschungsbericht 10402615, BRD, 221 pp.

Van der Salm, C. Weathering in forest soils, 1999. PhD Thesis, University of Amsterdam, Amsterdam, Netherlands, 288 pp.

Van Grinsven, J.J.M, N. van Breemen and J. Mulder, 1987. Impacts of acid atmospheric deposition on woodland soils in the Netherlands: I Calculation of hydrological and chemical budgets. Soil Sci. Soc. Am. Proc. 51: 1629-1634.

Vanmechelen, L., R. Groenemans and E. van Ranst, 1997. Forest soil condition in Europe. EC-UN/ECE, Brussels, Geneva, 257 pp.

Van Wallenburg, C., 1988. De dichtheid van moerige gronden. Wageningen, Netherlands Soil Survey Institute. Internal Report, 5 pp.

Annex 1 FAO soil types in Europe

A	ACRISOL	K	KASTANOZEM
Af	Ferric Acrisol	Kh	Haplic Kastanozem
Ag	Gleyic Acrisol	Khb	Vermi-Haplic Kastanozem
Ah	Humic Acrisol	Kk	Calcic Kastanozem
Ao	Orthic Acrisol	Kkb	Vermi-Calcic Kastanozem
Ap	Plinthic Acrisol	Kkv	Verti-Calcic Kastanozem
		Kl	Luvic Kastanozem
B	CAMBISOL	Ko	Orthic Kastanozem
Ba	Calcaric Cambisol		
Bc	Chromic Cambisol	L	LUVISOL
Bcc	Calcaro-Chromic Cambisol	La	Albic Luvisol
Bch	Humo-Chromic Cambisol	Lap	Plano-Albic Luvisol
Bck	Calci-Chromic Cambisol	Lc	Chromic Luvisol
Bd	Dystric Cambisol	Lcp	Plano-Chromic Luvisol
Bda	Ando-Dystric Cambisol	Lcr	Rhodo-Chromic Luvisol
Bdg	Gleyo-Dystric Cambisol	Lcv	Verti-Chromic Luvisol
Bds	Spodo-Dystric Cambisol	Ld	Dystric Luvisol
Be	Eutric Cambisol	Ldg	Gleyo-Dystric Luvisol
Bea	Ando-Eutric Cambisol	Lf	Ferric Luvisol
Bec	Calcaro-Eutric Cambisol	Lg	Gleyic Luvisol
Bef	Fluvi-Eutric Cambisol	Lga	Albo-Gleyic Luvisol
Beg	Gleyo-Eutric Cambisol	Lgp	Plano-Gleyic Luvisol
Bev	Verti-Eutric Cambisol	Lgs	Stagno-Gleyic Luvisol
Bg	Gleyic Cambisol	Lh	Humic Luvisol
Bgc	Calcaro-Gleyic Cambisol	Lk	Calcic Luvisol
Bge	Eutri-Gleyic Cambisol	Lkc	Chromo-Calcic Luvisol
Bgg	Stagno-Gleyic Cambisol	Lkcr	Rhodo-Chromo-Calcic Luvisol
Bgs	Spodo-Gleyic Cambisol	Lkv	Verti-Calcic Luvisol
Bh	Humic Cambisol	Lo	Orthic Luvisol
Bhc	Calcaro-Humic Cambisol	Lop	Plano-Orthic Luvisol
Bk	Calcic Cambisol	Lp	Plinthic Luvisol
Bkf	Fluvi-Calcic Cambisol	Ls	Spodic Luvisol
Bkh	Humo-Calcic Cambisol	Lv	Vertic Luvisol
Bkv	Verti-Calcic Cambisol	Lvc	Chromo-Vertic Luvisol
Bv	Vertic Cambisol	Lvcr	Rhodo-Chromo-Vertic Luvisol
Bvc	Calcaro-Vertic Cambisol	Lvk	Calci-Vertic Luvisol
Bvg	Gleyo-Vertic Cambisol		
Bvk	Calci-Vertic Cambisol	M	GREYZEM
Bx	Gelic Cambisol	Mo	Orthic Greyzem
Bxs	Spodo-Gelic Cambisol		
		O	HISTOSOL
C	CHERNOZEM	Od	Dystric Histosol
Ch	Haplic Chernozem	Odp	Placi-Dystric Histosol
Chp	Pachi-Haplic Chernozem	Oe	Eutric Histosol
Chv	Verti-Haplic Chernozem	Ox	Gelic Histosol
Ck	Calcic Chernozem		
Ckb	Vermi-Calcic Chernozem	P	PODZOL
Ckc	Calcaro-Calcic Chernozem	Pf	Ferric Podzol
Ckcb	Vermi-Calcaro-Calcic Chernozem	Pg	Gleyic Podzol
Ckcp	Pachi-Calcic Chernozem	Pgh	Histo-Gleyic Podzol
Cl	Luvic Chernozem	Pgs	Stagno-Gleyic Podzol
		Ph	Humic Podzol

D	PODZOLUVISOL	Phf	Ferro-Humic Podzol
Dd	Dystric Podzoluvisol	Pl	Leptic Podzol
De	Eutric Podzoluvisol	Plh	Humo-Leptic Podzol
Dg	Gleyic Podzoluvisol	Po	Orthic Podzol
Dgd	Dystric Gleyic Podzoluvisol	Pof	Ferro-Orthic Podzol
Dge	Eutric Gleyic Podzoluvisol	Poh	Humo-Orthic Podzol
Dgs	Stagno-Gleyic Podzoluvisol	Pol	Lepto-Orthic Podzol
		Pp	Placic Podzol
E	RENDZINA	Pph	Humo-Placic Podzol
Ec	Cambic Rendzina		
Eh	Histic Rendzina	Q	ARENOSOL
Eo	Orthic Rendzina	Qa	Albic Arenosol
		Qc	Cambic Arenosol
F	FERRALSOL	Qcc	Calcaro-Cambic Arenosol
Fo	Orthic Ferralsol	Qcd	Dystri-Cambic Arenosol
		Qcg	Gleyo-Cambic Arenosol
G	GLEYSOL	Qcs	Spodo-Cambic Arenosol
Gc	Calcaric Gleysol	Ql	Luvic Arenosol
Gcf	Fluvi-Calcaric Gleysol	Qld	Dystri-Luvic Arenosol
Gcs	Stagno-Calcaric Gleysol	Qlg	Gleyo-Luvic Arenosol
Gd	Dystric Gleysol		
Gdf	Fluvi-Dystric Gleysol	R	REGOSOL
Gds	Stagno-Dystric Gleysol	Rc	Calcaric Regosol
Ge	Eutric Gleysol	Rd	Dystric Regosol
Gef	Fluvi-Eutric Gleysol	Re	Eutric Regosol
Ges	Stagno-Eutric Gleysol		
Gev	Verti-Eutric Gleysol	S	OLONETZ
Gf	Fluvisol	Sg	Gleyic Solonetz
Gfm	Molli-Fluvisol	Sm	Mollic Solonetz
Gh	Humic Gleysol	So	Orthic Solonetz
Ghf	Fluvi-Humic Gleysol	Sof	Fluvi-Orthic Solonetz
Ghh	Histo-Humic Gleysol		
Ght	Thioni-Humic Gleysol	T	ANDOSOL
Gi	Histic Gleysol	Th	Humic Andosol
Gih	Humo-Histic Gleysol	Tm	Mollic Andosol
Gl	Luvic Gleysol	To	Ochric Andosol
Gls	Stagno-Luvic Gleysol	Tv	Vitric Andosol
Gm	Mollic Gleysol		
Gmc	Calcaro-Mollic Gleysol	U	RANKER
Gmf	Fluvi-Mollic Gleysol	Ud	Dystric Ranker
Gmv	Verti-Mollic Gleysol	Ul	Luvic Ranker
Gs	Stagnic Gleysol		
Gt	Thionic Gleysol	V	VERTISOL
		Vc	Chromic Vertisol
H	PHAEZEM	Vcc	Calcaro-Chromic Vertisol
Hc	Calcaric Phaeozem	Vg	Gleyic Vertisol
Hcf	Fluvi-Calcaric Phaeozem	Vp	Pellic Vertisol
Hcn	Alkalino-Calcaric Phaeozem	Vpc	Calcaro-Pellic Vertisol
Hcs	Saline-Calcaric Phaeozem	Vpg	Gleyo-Pellic Vertisol
Hg	Gleyic Phaeozem	Vpn	Sodi-Pellic Vertisol
Hgc	Calcaro-Gleyic Phaeozem		
Hgf	Fluvi-Gleyic Phaeozem	W	PLANOSOL
Hgs	Stagno-Gleyic Phaeozem	Wd	Dystric Planosol
Hgv	Verti-Gleyic Phaeozem	Wdv	Verti-Dystric Planosol

Hh	Haplic Phaeozem	We	Eutric Planosol
Hhv	Verti-Haplic Phaeozem	Wev	Verti-Eutric Planosol
Hl	Luvic Phaeozem	Wm	Mollic Planosol
Hlv	Verti-Luvic Phaeozem		
Ho	Orthic Phaeozem	X	XEROSOL
		Xk	Calcic Xerosol
I	Lithosol	Xl	Luvic Xerosol
Ic	Calcaric Lithosol	Xy	Gypsic Xerosol
Ich	Humo-Calcaric Lithosol		
Id	Dystric Lithosol	Z	SOLONCHAK
Ie	Eutric Lithosol	Zg	Gleyic Solonchak
		Zgf	Fluvi-Gleyic Solonchak
J	FLUVISOL	Zo	Orthic Solonchak
Jc	Calcaric Fluvisol	Zt	Takyric Solonchak
Jcf	Fluvi-Calcaric Fluvisol		
Jcg	Gleyo-Calcaric Fluvisol		
Jd	Dystric Fluvisol		
Jdf	Fluvi-Dystric Fluvisol		
Jdg	Gleyo-Dystric Fluvisol		
Je	Eutric Fluvisol		
Jef	Fluvi-Eutric Fluvisol		
Jeg	Gleyo-Eutric Fluvisol		
Jm	Mollic Fluvisol		
Jmg	Gleyo-Mollic Fluvisol		
Jmv	Verti-Mollic Fluvisol		
Jt	Thionic Fluvisol		

Annex 2 Site quality estimates

Site quality was derived from drainage status, fertility status and water availability. Each of these parameters was classified from poor (class 3) to good (class 1):

Drainage status:

Class	Description
1	moderately well or better
2	temporary poor
3	poor or very poor

Fertility status

Class	Description
1	C/N < 21
2	C/N 21 - 33
3	C/N > 33

Water availability class

AWC (mm)	< 75	75-175	> 175
Precipitation deficit (mm)			
0-100	2	1	1
100-300	3	2	1
> 300	3	3	2

Finally quality estimates for the separate parameters are combined into one site quality index. The site quality is reduced by 1 class for acid soils (Podzols, Arenosols and all dystric soils) to account for the negative effects of acidity on site quality.

Site quality estimates

Nutrients	1			2			3		
Water	1	2	3	1	2	3	1	2	3
Drainage									
1	1	2	2	2	2	3	2	3	3
2	2	2	3	2	3	3	3	3	3
3	3	3	3	3	3	3	3	3	3

Annex 3 Yield tables

Species group definition

Group code	Group name	Leading species	ICP Forest species included (by number)
Con_1	Pine	134	<i>Pinus sylvestris</i> 123, 124, 128, 129, 133, 134, 135
Con_2	Spruce	118	<i>Picea abies</i> 100, 101, 102, 103, 104, 105, 106, 118, 119, 120, 136, 139
Con_3	Larch	116	<i>Larix decidua</i> 116, 117
Con_4	Cedar	107	<i>Cedrus atlantica</i> 107, 108, 121, 122, 125, 126, 127, 130, 131, 132
Con_5	Cypress	110	<i>Cupressus sempervirens</i> 109, 110, 111, 112, 113, 114, 115, 137, 138, 140, 199
Dec_1	Oak	051	<i>Quercus robur</i> 1, 2, 3, 4, 5, 16, 27, 36, 37, 38, 40, 41, 42, 43, 44, 45, 47, 48, 49, 50, 51, 53, 56, 99
Dec_2	Beech	020	<i>Fagus sylvatica</i> 13, 14, 15, 18, 19, 20, 26, 27, 29, 30, 68, 69, 70, 71, 72
Dec_3	Evergr. Broadleaves	046	<i>Quercus ilex</i> 24, 28, 46, 52, 54, 55, 73, 74, 80, 81, 82, 83
Dec_4	Poplar	033	<i>Populus hybrides</i> 17, 21, 22, 23, 31, 32, 33, 34, 35, 57, 58, 59, 60, 61, 62
Dec_5	Birch	010	<i>Betula pendula</i> 6, 7, 8, 9, 10, 11, 12, 39, 63, 64, 65, 66, 67, 75, 76, 77, 78, 79, 84, 85, 86, 87, 88, 89, 90

Climate zone definition

Code	Climatic zone
AN	Atlantic north
AS	Atlantic south
B	Boreal
BN	Boreal > 65.00 latitude
BT	Boreal temperate
C	Continental
MH	Mediterranean higher (500 -1000 m)
ML	mediterranean lower
MN	mountainous north
MNN	mountainous north > 65.00 latitude
MS	mountainous 'south' (1000 - 1500 m)
MSA	mountainous 'south' high elevation (> 1500 m)
S	subatlantic

Yield classes as a function of species group, climate zone and site quality (SQ; H=High,M=Medium,L=Low);

Species group	Climate zone	SQ	Yield class	Species group	Climate zone	SQ	Yield class
Con_1	AN	H	12	Dec_1	AN	H	8
Con_1	AN	L	4	Dec_1	AN	L	4
Con_1	AN	M	8	Dec_1	AN	M	6
Con_1	AS	H	12	Dec_1	AS	H	8
Con_1	AS	L	4	Dec_1	AS	L	4
Con_1	AS	M	8	Dec_1	AS	M	6
Con_1	B	H	6	Dec_1	B	H	4
Con_1	B	L	2	Dec_1	B	L	0
Con_1	B	M	4	Dec_1	B	M	2
Con_1	BN	H	4	Dec_1	BN	H	0

Con_1	BN	L	0	Dec_1	BN	L	0
Con_1	BN	M	2	Dec_1	BN	M	0
Con_1	BT	H	10	Dec_1	BT	H	8
Con_1	BT	L	4	Dec_1	BT	L	2
Con_1	BT	M	6	Dec_1	BT	M	4
Con_1	C	H	10	Dec_1	C	H	6
Con_1	C	L	4	Dec_1	C	L	4
Con_1	C	M	8	Dec_1	C	M	6
Con_1	MH	H	12	Dec_1	MH	H	6
Con_1	MH	L	2	Dec_1	MH	L	2
Con_1	MH	M	6	Dec_1	MH	M	4
Con_1	ML	H	12	Dec_1	ML	H	8
Con_1	ML	L	4	Dec_1	ML	L	4
Con_1	ML	M	8	Dec_1	ML	M	6
Con_1	MN	H	8	Dec_1	MN	H	4
Con_1	MN	L	4	Dec_1	MN	L	2
Con_1	MN	M	6	Dec_1	MN	M	2
Con_1	MNN	H	6	Dec_1	MNN	H	4
Con_1	MNN	L	2	Dec_1	MNN	L	0
Con_1	MNN	M	4	Dec_1	MNN	M	2
Con_1	MS	H	12	Dec_1	MS	H	8
Con_1	MS	L	4	Dec_1	MS	L	4
Con_1	MS	M	8	Dec_1	MS	M	6
Con_1	MSA	H	8	Dec_1	MSA	H	6
Con_1	MSA	L	4	Dec_1	MSA	L	4
Con_1	MSA	M	6	Dec_1	MSA	M	4
Con_1	S	H	12	Dec_1	S	H	8
Con_1	S	L	4	Dec_1	S	L	4
Con_1	S	M	8	Dec_1	S	M	6
Con_2	AN	H	20	Dec_2	AN	H	10
Con_2	AN	L	6	Dec_2	AN	L	4
Con_2	AN	M	10	Dec_2	AN	M	6
Con_2	AS	H	16	Dec_2	AS	H	12
Con_2	AS	L	6	Dec_2	AS	L	4
Con_2	AS	M	10	Dec_2	AS	M	8
Con_2	B	H	8	Dec_2	B	H	0
Con_2	B	L	2	Dec_2	B	L	0
Con_2	B	M	6	Dec_2	B	M	0
Con_2	BN	H	6	Dec_2	BN	H	0
Con_2	BN	L	0	Dec_2	BN	L	0
Con_2	BN	M	4	Dec_2	BN	M	0
Con_2	BT	H	10	Dec_2	BT	H	4
Con_2	BT	L	4	Dec_2	BT	L	2
Con_2	BT	M	6	Dec_2	BT	M	2
Con_2	C	H	12	Dec_2	C	H	10
Con_2	C	L	6	Dec_2	C	L	4
Con_2	C	M	8	Dec_2	C	M	6
Con_2	MH	H	10	Dec_2	MH	H	12
Con_2	MH	L	4	Dec_2	MH	L	4

Con_2	MH	M	6	Dec_2	MH	M	6
Con_2	ML	H	12	Dec_2	ML	H	10
Con_2	ML	L	4	Dec_2	ML	L	4
Con_2	ML	M	8	Dec_2	ML	M	6
Con_2	MN	H	12	Dec_2	MN	H	0
Con_2	MN	L	4	Dec_2	MN	L	0
Con_2	MN	M	6	Dec_2	MN	M	0
Con_2	MNN	H	8	Dec_2	MNN	H	0
Con_2	MNN	L	2	Dec_2	MNN	L	0
Con_2	MNN	M	4	Dec_2	MNN	M	0
Con_2	MS	H	10	Dec_2	MS	H	10
Con_2	MS	L	6	Dec_2	MS	L	4
Con_2	MS	M	8	Dec_2	MS	M	6
Con_2	MSA	H	8	Dec_2	MSA	H	8
Con_2	MSA	L	4	Dec_2	MSA	L	4
Con_2	MSA	M	6	Dec_2	MSA	M	6
Con_2	S	H	12	Dec_2	S	H	12
Con_2	S	L	6	Dec_2	S	L	4
Con_2	S	M	8	Dec_2	S	M	8
Con_3	AN	H	12	Dec_3	AN	H	0
Con_3	AN	L	4	Dec_3	AN	L	0
Con_3	AN	M	8	Dec_3	AN	M	0
Con_3	AS	H	14	Dec_3	AS	H	4
Con_3	AS	L	4	Dec_3	AS	L	2
Con_3	AS	M	8	Dec_3	AS	M	4
Con_3	B	H	4	Dec_3	B	H	0
Con_3	B	L	0	Dec_3	B	L	0
Con_3	B	M	2	Dec_3	B	M	0
Con_3	BN	H	0	Dec_3	BN	H	0
Con_3	BN	L	0	Dec_3	BN	L	0
Con_3	BN	M	0	Dec_3	BN	M	0
Con_3	BT	H	8	Dec_3	BT	H	0
Con_3	BT	L	2	Dec_3	BT	L	0
Con_3	BT	M	4	Dec_3	BT	M	0
Con_3	C	H	8	Dec_3	C	H	4
Con_3	C	L	4	Dec_3	C	L	2
Con_3	C	M	6	Dec_3	C	M	4
Con_3	MH	H	8	Dec_3	MH	H	6
Con_3	MH	L	4	Dec_3	MH	L	2
Con_3	MH	M	6	Dec_3	MH	M	4
Con_3	ML	H	8	Dec_3	ML	H	8
Con_3	ML	L	2	Dec_3	ML	L	2
Con_3	ML	M	4	Dec_3	ML	M	4
Con_3	MN	H	6	Dec_3	MN	H	0
Con_3	MN	L	2	Dec_3	MN	L	0
Con_3	MN	M	4	Dec_3	MN	M	0
Con_3	MNN	H	0	Dec_3	MNN	H	0
Con_3	MNN	L	0	Dec_3	MNN	L	0
Con_3	MNN	M	0	Dec_3	MNN	M	0

Con_3	MS	H	14	Dec_3	MS	H	6
Con_3	MS	L	6	Dec_3	MS	L	2
Con_3	MS	M	10	Dec_3	MS	M	4
Con_3	MSA	H	8	Dec_3	MSA	H	6
Con_3	MSA	L	4	Dec_3	MSA	L	2
Con_3	MSA	M	6	Dec_3	MSA	M	4
Con_3	S	H	8	Dec_3	S	H	6
Con_3	S	L	4	Dec_3	S	L	2
Con_3	S	M	6	Dec_3	S	M	4
Con_4	AN	H	6	Dec_4	AN	H	16
Con_4	AN	L	2	Dec_4	AN	L	8
Con_4	AN	M	4	Dec_4	AN	M	12
Con_4	AS	H	14	Dec_4	AS	H	20
Con_4	AS	L	4	Dec_4	AS	L	12
Con_4	AS	M	8	Dec_4	AS	M	16
Con_4	B	H	0	Dec_4	B	H	4
Con_4	B	L	0	Dec_4	B	L	0
Con_4	B	M	0	Dec_4	B	M	0
Con_4	BN	H	0	Dec_4	BN	H	0
Con_4	BN	L	0	Dec_4	BN	L	0
Con_4	BN	M	0	Dec_4	BN	M	0
Con_4	BT	H	0	Dec_4	BT	H	8
Con_4	BT	L	0	Dec_4	BT	L	0
Con_4	BT	M	0	Dec_4	BT	M	4
Con_4	C	H	6	Dec_4	C	H	16
Con_4	C	L	2	Dec_4	C	L	4
Con_4	C	M	4	Dec_4	C	M	8
Con_4	MH	H	14	Dec_4	MH	H	16
Con_4	MH	L	4	Dec_4	MH	L	4
Con_4	MH	M	10	Dec_4	MH	M	12
Con_4	ML	H	14	Dec_4	ML	H	16
Con_4	ML	L	4	Dec_4	ML	L	4
Con_4	ML	M	8	Dec_4	ML	M	8
Con_4	MN	H	0	Dec_4	MN	H	4
Con_4	MN	L	0	Dec_4	MN	L	0
Con_4	MN	M	0	Dec_4	MN	M	4
Con_4	MNN	H	0	Dec_4	MNN	H	0
Con_4	MNN	L	0	Dec_4	MNN	L	0
Con_4	MNN	M	0	Dec_4	MNN	M	0
Con_4	MS	H	6	Dec_4	MS	H	12
Con_4	MS	L	2	Dec_4	MS	L	4
Con_4	MS	M	4	Dec_4	MS	M	8
Con_4	MSA	H	4	Dec_4	MSA	H	8
Con_4	MSA	L	0	Dec_4	MSA	L	0
Con_4	MSA	M	0	Dec_4	MSA	M	4
Con_4	S	H	8	Dec_4	S	H	16
Con_4	S	L	2	Dec_4	S	L	8
Con_4	S	M	4	Dec_4	S	M	12
Con_5	AN	H	10	Dec_5	AN	H	8

Con_5	AN	L	4	Dec_5	AN	L	4
Con_5	AN	M	6	Dec_5	AN	M	6
Con_5	AS	H	16	Dec_5	AS	H	8
Con_5	AS	L	4	Dec_5	AS	L	4
Con_5	AS	M	10	Dec_5	AS	M	6
Con_5	B	H	0	Dec_5	B	H	4
Con_5	B	L	0	Dec_5	B	L	2
Con_5	B	M	0	Dec_5	B	M	4
Con_5	BN	H	0	Dec_5	BN	H	2
Con_5	BN	L	0	Dec_5	BN	L	0
Con_5	BN	M	0	Dec_5	BN	M	2
Con_5	BT	H	4	Dec_5	BT	H	4
Con_5	BT	L	0	Dec_5	BT	L	2
Con_5	BT	M	2	Dec_5	BT	M	4
Con_5	C	H	12	Dec_5	C	H	6
Con_5	C	L	4	Dec_5	C	L	4
Con_5	C	M	8	Dec_5	C	M	6
Con_5	MH	H	12	Dec_5	MH	H	6
Con_5	MH	L	4	Dec_5	MH	L	2
Con_5	MH	M	8	Dec_5	MH	M	4
Con_5	ML	H	16	Dec_5	ML	H	6
Con_5	ML	L	6	Dec_5	ML	L	2
Con_5	ML	M	12	Dec_5	ML	M	4
Con_5	MN	H	0	Dec_5	MN	H	4
Con_5	MN	L	0	Dec_5	MN	L	2
Con_5	MN	M	0	Dec_5	MN	M	4
Con_5	MNN	H	0	Dec_5	MNN	H	4
Con_5	MNN	L	0	Dec_5	MNN	L	0
Con_5	MNN	M	0	Dec_5	MNN	M	2
Con_5	MS	H	10	Dec_5	MS	H	6
Con_5	MS	L	2	Dec_5	MS	L	4
Con_5	MS	M	6	Dec_5	MS	M	4
Con_5	MSA	H	2	Dec_5	MSA	H	4
Con_5	MSA	L	0	Dec_5	MSA	L	2
Con_5	MSA	M	0	Dec_5	MSA	M	4
Con_5	S	H	12	Dec_5	S	H	6
Con_5	S	L	4	Dec_5	S	L	4
Con_5	S	M	8	Dec_5	S	M	6

Average stem-increment estimates (in m³.ha⁻¹.yr⁻¹) as a function of species group and yield class

Species group	Yield class	Stem-Increment	Species group	Yield class	Stem-Increment
Con_1	0	1.2	Dec_1	0	1.0
Con_1	2	2.3	Dec_1	2	2.0
Con_1	4	4.0	Dec_1	4	4.0
Con_1	6	6.0	Dec_1	6	6.0
Con_1	8	8.0	Dec_1	8	8.0
Con_1	10	10.0	Dec_2	0	1.0
Con_1	12	12.0	Dec_2	2	1.9
Con_2	0	1.0	Dec_2	4	4.0
Con_2	2	2.0	Dec_2	6	6.0
Con_2	4	4.0	Dec_2	8	8.0
Con_2	6	6.0	Dec_2	10	10.0
Con_2	8	8.0	Dec_2	12	12.0
Con_2	10	10.0	Dec_3	0	0.7
Con_2	12	12.0	Dec_3	2	1.4
Con_2	16	16.0	Dec_3	4	2.8
Con_2	20	20.0	Dec_3	6	4.2
Con_3	0	1.0	Dec_3	8	5.6
Con_3	2	2.0	Dec_4	0	2.0
Con_3	4	4.0	Dec_4	4	4.0
Con_3	6	6.0	Dec_4	8	8.0
Con_3	8	8.0	Dec_4	12	11.5
Con_3	10	10.0	Dec_4	16	16.8
Con_3	12	12.0	Dec_4	20	20.0
Con_3	14	14.0	Dec_5	0	1.0
Con_4	0	1.2	Dec_5	2	2.0
Con_4	2	2.3	Dec_5	4	4.0
Con_4	4	4.0	Dec_5	6	6.0
Con_4	6	6.0	Dec_5	8	8.0
Con_4	8	8.0			
Con_4	10	10.0			
Con_4	12	12.0			
Con_4	14	14.0			
Con_5	0	1.0			
Con_5	2	2.0			
Con_5	4	4.0			
Con_5	6	6.0			
Con_5	8	8.0			
Con_5	10	10.0			
Con_5	12	12.0			
Con_5	16	16.0			

Annex 4 Evapotranspiration and Soil Moisture Calculations

Here we summarize the equations of the model used for calculating evapotranspiration and soil moisture. The model is essentially the same as used in the IMAGE global change model (Leemans and van den Born, 1994); it follows the approach by Prentice et al. (1993).

Soil moisture:

Soil moisture is modeled in a very simple way, assuming a single water store from which runoff occurs only when the store is full. Snow and soil frost are not modeled. Soil moisture on day i , O_i (in mm), is given by:

$$\Omega_i = \min\{\max\{0, \Omega_{i-1} + (P_i - E_i)\Delta t\}, \Omega_{\max}\} \quad (1)$$

where P_i and E_i are the precipitation (mm/day) and actual evapotranspiration (mm/day), resp., on day i , $t=1$ day, and Ω_{\max} is the soil water capacity (field capacity minus wilting point, in mm). O_1 is initialized with $1/3 P_a$ (P_a = annual precipitation), and eq.1 is iterated as long as $|O_{365} - O_1| > 2\text{mm}$ (but max. thrice).

Actual evapotranspiration (AET):

AET is calculated by a method based on Federer (1982). The *instantaneous* AET, E , is the lesser of the supply S and the demand D :

$$E = \min\{S, D\} \quad (2)$$

To obtain the AET for day i one has to integrate over that day. Assuming $t=0$ for noon, we have:

$$E_i = \int_{-t_e}^{t_e} \min\{S(t), D(t)\} dt \quad (3)$$

where $[-t_e, t_e]$ is one day. Following Federer (1982),

$$S = c_w (\Omega_{i-1} / \Omega_{\max}) \quad (4)$$

i.e. the supply is proportional to relative soil wetness, which does not change significantly during the day; and c_w is the maximum evapotranspiration rate from saturated soils ($c_w=1\text{mm/h}$). The demand D on the other hand changes during the course of a day as a function of the Sun's elevation; it has the general form

$$D(t) = \max\{U + V \cos(\omega t), 0\} \quad (5)$$

where U and $V \geq 0$ are independent of the time of the day (we suppress the day-index i for convenience); and $\omega = 2\pi/24$ if t is measured in hours, $\omega = 2\pi/(24 \cdot 60)$ if t is measured in minutes, etc. Thus eq.3 becomes

$$E_i = 2 \int_0^{t_e} \min\{ S, \max\{ U + V \cos(\omega t), 0 \} \} dt \quad (6)$$

where we have made use of the fact that the cosine is symmetric around $t=0$ (noon). To evaluate the integral in eq.6 we first assume that the supply S is not limiting, i.e. $S > U + V$. We then have $E_i = D_i$ which is given by (see grey-shaded area in Fig.A):

$$D_i = 2 \int_0^{t_e} \min\{ U + V \cos(\omega t), 0 \} dt = \frac{2V}{\omega} f(U/V) \quad (7)$$

with

$$f(x) = \begin{cases} 0 & \text{for } x < -1 \\ x \arccos(-x) + \sqrt{1-x^2} & \text{for } -1 \leq x \leq 1 \\ px & \text{for } x > 1 \end{cases} \quad (8)$$

Observing that $\min\{y, \max\{x, 0\}\} = \max\{x, 0\} - \max\{x-y, 0\}$ for all $y \geq 0$, we obtain for arbitrary $S \geq 0$ by using eq.7 twice:

$$E_i = \frac{2V}{\omega} [f(U/V) - f((U-S)/V)] \quad (9)$$

Potential evapotranspiration (PET):

Following the theory of equilibrium evapotranspiration (see Jarvis and McNaughton 1986) we equate instantaneous evaporative demand D with the equilibrium evapotranspiration rate (in mm/h):

$$D(t) = \frac{3600}{Lr} \frac{s}{s+g} R_n \quad (10)$$

where L is the latent heat of vaporization of water, ρ is the density of water ($=1 \text{ kg}/(\text{m}^3 \cdot \text{mm})$), s is the rate of change of the saturated vapor pressure with temperature, γ is the psychrometric constant, R_n is the instantaneous net radiation (W/m^2), and the factor 3600 converts from seconds to hours. Both L and γ depend weakly on temperature: between -5°C and $+45^\circ\text{C}$ they vary linearly with temperature between 2.513 and 2.394 MJ/kg and between 64.6 and 67.8 Pa/K, resp. The dependence of s on the temperature T (in $^\circ\text{C}$) is given by (Priestley and Taylor, 1972):

$$s = c_1 c_2 c_3 \frac{\exp[c_2 T / (c_3 + T)]}{(c_3 + T)^2} \text{ Pa/K} \quad (11)$$

with $c_1 = 610.78 \text{ Pa}$, $c_2 = 17.269$, $c_3 = 237.3 \text{ K}$

The net radiation R_n is the difference between the net downward short-wave flux R_s and the net upward long-wave flux R_l . Following Linacre (1968) we take

$$R_s = (c + dn_i)(1 - b)s[1 + 2e \cos(2\pi i / 365)] \cos z \quad (12)$$

where n_i is the fraction of sunshine on day i , $c=0.25$ and $d=0.5$ are empirical constants ($c+d$ is the clear-sky transmissivity), b is the short-wave albedo, $s=1360\text{W/m}^2$ is the solar constant, $e=0.01675$ is the Earth's orbital eccentricity, and

$$\cos z = \sin \phi \sin \delta + \cos \phi \cos \delta \cos(\omega t) \quad (13)$$

where ϕ is latitude, and

$$\delta = -23.4^\circ \cos[2\pi(i + 10) / 365] \quad (24)$$

The net upward long-wave flux is approximated by a linear function of the temperature T (in $^\circ\text{C}$). Again following Linacre (1968),

$$R_l = [b + (1 - b)n_i](A - T) \quad (15)$$

where $b=0.2$ and $A=107\text{K}$ are empirical constants. Taking T as the mean daily temperature we neglect the effects of diurnal temperature variations on s , ϕ , L and R_l . D is then a linear function of $\cos(\omega t)$ (as in eq.5) and the daily equilibrium evapotranspiration D_i is given by eq.7.

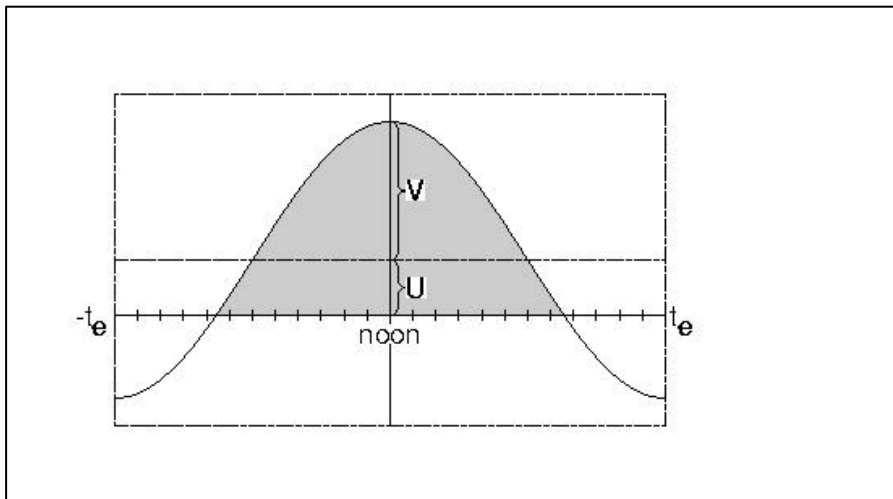


Figure A: Cosine-shaped demand function (potential evapotranspiration) for a given day (see eq. 5)

